

Convergence and Applications of the Implicit Finite Difference Method for Advection-Diffusion-Reaction Equations

Kanokwan Pananu, Surattana Sungnul, Sekson Sirisubtawee and Sutthisak Phongthanapanich

Abstract—In this paper, we analyze the convergence of the finite difference method with the implicit forward time central space (FTCS) scheme for the two-dimensional advection-diffusion-reaction equation (ADRE). It is discovered that the method is unconditionally convergent. The validation of the scheme is verified with a 1-D ADRE. We apply the scheme to a pollutant dispersion with removal mechanism model in a reservoir. The number of entrance gates, the decreasing rate of water pollutant and the dispersion coefficient are varied in our problem to obtain numerical solutions. Graphical representations of the obtained solutions are demonstrated. As a numerical result, we find that the water pollutant concentration of the problem depends upon the number of entrance gates, the decreasing rate of water pollutant and the dispersion coefficient.

Index Terms—Water pollutant concentration, Finite difference method, Convergence, Advection-diffusion-reaction equation, Implicit FTCS scheme

I. INTRODUCTION

THE advection-diffusion-reaction equation (ADRE) has been widely used as a mathematical model in many different areas of the sciences and engineering. Accurate numerical solutions of the ADRE play an important role in simulations for a large class of physical systems. There are now many different numerical methods that have been developed to solve linear and nonlinear ADREs. For example, finite difference methods (FDM) (see, e.g., [1]–[11], finite element methods (FEM) [12], finite volume methods (FVM) (see, e.g., [13]–[17]) and meshless methods (see, e.g., [18]–[22]).

In particular, many researchers have used the schemes involving with the finite difference method to numerically solve equations associated with the ADRE as follows. For example, in 2009, Feng [1] proposed an integral form of convection-diffusion equation and constructed a class of alternating group explicit finite difference method (AGE) based

on several asymmetric schemes. The method is unconditionally stable. In 2010, Siddique [23] employed Padé schemes to obtain the numerical solutions of two-dimensional (both homogeneous and inhomogeneous) diffusion equations subject to nonlocal boundary conditions. The obtained numerical results demonstrated the accuracy of these schemes. In 2011, Prieto et al. [2] applied a generalized explicit finite difference method to solve advection-diffusion equations and studied the convergence of the method. In 2013, Chen-Charpentier and Kojouharov [3] proposed the unconditionally positive finite-difference (UPFD) method to solve parabolic equations with advection, diffusion, and reaction terms for positive solutions. The method is independent of the time step and mesh size. Appadu [4] compared the numerical solutions of the 1-D advection-diffusion equation with constant coefficients obtained using the three numerical methods including the Lax-Wendroff, the Crank-Nicolson and nonstandard finite difference schemes. In 2014, Kaya [5] proposed a finite difference scheme for multidimensional convection-diffusion-reaction equations. Particularly, the scheme was designed to treat the most interesting case of small diffusion. Zhang et al. [6] proposed an exact finite difference scheme using the solitary wave solutions to solve Burgers and Burgers-Fisher equations. In 2015, Kaya [7] studied the numerical solution of multidimensional unsteady convection-diffusion-reaction equations using finite difference method on a special grid. The method gives good performance for the numerical tests. Kaya and Sendur [8] proposed a finite difference method on a special grid for solving the convection-diffusion-reaction (CDR) problems with small diffusion and compared the performance of the proposed method with the Streamline-upwind Petrov-Galerkin (SUPG) and the Residual-Free Bubbles (RFB) methods on several benchmark problems. In 2017, Sanjaya and Mungkasi [9] investigated the performance of an explicit finite difference method for solving one dimension the advection-diffusion equation. Kewalee and Nopparat [10] studied the air quality model in areas under a Bangkok sky train platform via a three-dimensional advection-diffusion equation with time dependence. The model was solved for numerical solutions using the explicit forward difference in time and central difference in space (FTCS). They also investigated the wind inflow for two cases: only in x -direction and in x - and y -directions. Moreover, some obstacles were included into the tunnel to study their effects on the numerical simulations. In 2018, Company et al. [11] utilized the positivity-preserving finite difference scheme to obtain solutions of multidimensional advection-diffusion-reaction problems. Qian and Cai [24] proposed the implicit-explicit time stepping stream-

Manuscript received February 27, 2020; revised May 2, 2020. This research was funded by the Science Achievement Scholarship of Thailand (SAST).

Kanokwan Pananu is Ph.D student in the Applied Mathematics, King Mongkut's University of Technology North Bangkok, 10800 THAILAND (e-mail: kanokwan.kanok@gmail.com).

Surattana Sungnul is currently lecturer at the Department of Mathematics, King Mongkut's University of Technology North Bangkok, 10800 THAILAND and researcher in Center of Excellence in Mathematics, 10400 THAILAND (corresponding author, e-mail: surattana.s@sci.kmutnb.ac.th).

Sekson Sirisubtawee is currently lecturer at the Department of Mathematics, King Mongkut's University of Technology North Bangkok, 10800 THAILAND and researcher in Center of Excellence in Mathematics, 10400 THAILAND (e-mail: sekson.s@sci.kmutnb.ac.th).

Sutthisak Phongthanapanich is currently lecturer at Department of Mechanical Engineering Technology, College of Industrial Technology, King Mongkut's University of Technology North Bangkok 10800 THAILAND (e-mail: sutthisak.p@cit.kmutnb.ac.th).

line diffusion method for numerically solving the fluid-fluid interaction problems modelled using the convection-dominated convection-diffusion-reaction equations with an interface condition. They analyzed the stability and error estimates of scheme as well.

In this article, we consider the advection-diffusion-reaction equation of the following form:

$$\frac{\partial \phi}{\partial t} + \nabla \cdot (\mathbf{v}\phi - \varepsilon \nabla \phi) + \kappa \phi = q, \quad (1)$$

where ϕ is a scalar quantity, $\mathbf{v} = \mathbf{v}(\mathbf{x})$ is a given advection velocity vector, $\varepsilon \geq 0$ is a diffusion coefficient, κ is a reaction coefficient, $q = q(\mathbf{x}, t)$ is a prescribed source term, \mathbf{x} is a position vector and time $t \in [0, T]$, where $T > 0$. The present paper is organized as follows. The convergence theory is briefly provided in section II. The convergence and validation of the method are given in section III and IV, respectively. Using the method, numerical results and their graphs for the water pollution problem in reservoir written in terms of the ADRE in Eq. (1) are shown in section V. The conclusion of our work is presented in section VI.

II. CONVERGENCE THEORY

Let $L : \Omega \rightarrow H$ be a linear differential operator acting from a space of continuous functions Ω to a continuous function space H . Next, we consider the initial time-space boundary value problem (IBVP) consisting of the partial differential equation, when D is an interior set of the spatial domain and $T > 0$,

$$L\phi(\mathbf{x}, t) = q(\mathbf{x}, t), \quad (\mathbf{x}, t) \in D \times (0, T], \quad (2)$$

and the following initial time condition

$$\phi(\mathbf{x}, 0) = \psi(\mathbf{x}) \quad \text{for } \mathbf{x} \in D, \quad (3)$$

and the boundary space condition

$$\phi(\mathbf{x}, t) = \xi(\mathbf{x}, t) \quad \text{for } (\mathbf{x}, t) \in \partial D \times [0, T], \quad (4)$$

where ∂D is the boundary of the spatial domain.

Then, we consider a rectangular region which has a width of L_1 and a length of L_2 and time $t \in [0, T]$. Let D_h and ∂D_h be the discretized versions of D and ∂D , respectively. We define the spatial grid $\bar{D}_h = D_h \cup \partial D_h \subset D \cup \partial D$ as

$$\bar{D}_h = \{(x_i, y_j) \in D \cup \partial D \mid (i, j) \in J\}, \quad (5)$$

where $J = \{(i, j) \mid i = 0, 1, 2, \dots, N_1, j = 0, 1, 2, \dots, N_2\}$, $N_1 = \frac{L_1}{\Delta x}$, $N_2 = \frac{L_2}{\Delta y}$, and $\Delta x, \Delta y$ are the spatial step sizes in the direction of x and y , respectively. For the sake of convenience, $\Delta x = \Delta y = h$. Similarly, the interval $[0, T]$ is discretized as $[0, T]_k$ in which $t_n, n \in K = \{0, 1, 2, \dots, N\}$ are the temporal grid points with the step size $\Delta t = T/N$ for some positive integer number N . We define the linear space of discrete functions Ω_h for space step sizes h and time step size k on the grid $\bar{D}_h \times [0, T]_k \subset D \cup \partial D \times [0, T]$ and then consider a finite difference scheme (FDS) corresponding to the above initial-boundary value problem (2) as follows

$$L_h \phi^h = q^h, \quad (\mathbf{x}, t) \in D_h \times (0, T]_k, \quad (6)$$

where $L_h : \Omega_h \rightarrow H_h$ is a difference operator acting from a discrete function space Ω_h to a discrete function space H_h subject to the initial condition

$$\phi^h(\mathbf{x}, 0) = \psi^h(\mathbf{x}), \quad \mathbf{x} \in D_h \quad (7)$$

and the boundary condition

$$\phi^h(\mathbf{x}, t) = \xi^h(\mathbf{x}, t) \quad \text{for } (\mathbf{x}, t) \in \partial D_h \times [0, T]_k, \quad (8)$$

We define the function f^h as

$$f^h = f_{i,j}^n = \begin{cases} q_{i,j}^n, & (i, j) \in J, n \in K - \{0\}, \\ \psi_{i,j}^0, & (i, j) \in J, \end{cases} \quad (9)$$

where $\phi_{i,j}^n = \phi(x_i, y_j, t_n)$, $q_{i,j}^n = q(x_i, y_j, t_n)$ and $\psi_{i,j}^0 = \psi(x_i, y_j, 0)$.

Introducing the norms in the sense of discrete functions as

$$\begin{aligned} \|\phi^h\|_{\Omega_h} &= \max_{\substack{i,j \in J \\ n \in K}} |\phi_{i,j}^n|, \\ \|f^h\|_{H_h} &= \max_{i,j \in J} |\psi_{i,j}^0| + \max_{\substack{i,j \in J \\ n \in K - \{0\}}} |q_{i,j}^n|, \end{aligned} \quad (10)$$

and defining $\mathcal{P}_h : \Omega \rightarrow \Omega_h$ as a projection operator, we have the definition of convergence for numerical methods as follows.

Definition 2.1: Convergence

A solution ϕ^h of FDS in Eq. (6)-(8) converges to the solution ϕ of IBVP in Eq. (2)-(4) if

$$\|\mathcal{P}_h(\phi) - \phi^h\|_{\Omega_h} \rightarrow 0 \quad \text{as } h \rightarrow 0. \quad (11)$$

Definition 2.2: Convergence with order m

The FDS in Eq. (6) converges with order m if

$$\|\mathcal{P}_h(\phi) - \phi^h\|_{\Omega_h} \leq Ch^m \quad (12)$$

where the positive constant C does not depend on h .

Given a properly posed boundary value problem and a finite difference approximation to it, the necessary and sufficient conditions for convergence of the finite difference method, i.e. Lax's equivalence theorem [25], are consistency and stability.

1) Consistency : A finite difference representation of a PDE is said to be consistent [25] if the difference between the PDE and its difference representation vanishes as the mesh is refined, i.e., the truncation error (T.E.) goes to zero as the mesh size goes to zero. This should always be the case if the order of the T.E. vanishes under grid refinement.

The FDS (6) approximates BVP (2) with order m if

$$\|T.E.\|_{H_h} \leq Ch^m$$

where the positive constant C does not depend on h .

2) Stability : The finite difference scheme defined by (6) with linear operator L_h will be called stable, if there exists $h_0 > 0$ such that for arbitrary $h < h_0$ and for any discrete function $f^h \in H_h$, the solution ϕ^h of FDS (6) exists and is unique and also satisfies the inequality

$$\|\phi^h\|_{\Omega_h} \leq C \|f^h\|_{H_h}, \quad (13)$$

where the positive constant C does not depend on h . In other words, the scheme (6) is called stable for $(\mathbf{x}, t) \in \bar{D}_h \times [0, T]_k$, if there exists a positive constant C which is independent of h such that

$$\max_{i,j,n} |\phi_{i,j}^n| \leq C (\max_{i,j} |\psi_{i,j}^0| + \max_{i,j,n} |q_{i,j}^n|), \quad (14)$$

where $(i, j) \in J, n \in K$. The inequality (14) has to be true for any functions $\psi_{i,j}^0$ and $q_{i,j}^n$. In particular, if $q_{i,j}^n = 0$, then

the condition (14) becomes only the necessary condition for stability of (6).

For the special case of Fourier or Von Neumann Analysis [25], a solution of the FDS (6) for $q_{i,j}^n = 0$ can be written in the form

$$\phi_{i,j}^n = \lambda^n(\alpha, \beta)e^{I(\alpha i + \beta j)}, \quad (i, j) \in J, \quad n \in K, \quad I = \sqrt{-1} \quad (15)$$

where α and β are wave numbers and $e^{I(\alpha i + \beta j)}$ are eigenvectors corresponding to eigenvalues $\lambda(\alpha, \beta)$ of L_h . The necessary condition for stability of FDS (6) for $q_{i,j}^n = 0$ will then hold for all $\alpha, \beta \in \mathbb{R}$ if the following inequality holds:

$$|\lambda(\alpha, \beta)| \leq 1. \quad (16)$$

III. CONSISTENCY AND STABILITY ANALYSIS

Consider the following initial-boundary value problem

$$\frac{\partial \phi}{\partial t} + \bar{u} \frac{\partial \phi}{\partial x} + \bar{v} \frac{\partial \phi}{\partial y} - \varepsilon \left(\frac{\partial^2 \phi}{\partial x^2} + \frac{\partial^2 \phi}{\partial y^2} \right) + \kappa \phi = q(x, y, t),$$

$$(x, y) \in (0, L_1) \times (0, L_2), \quad t \in (0, T],$$

subject to

$$\begin{aligned} \phi(x, y, 0) &= \psi(x, y), \\ \phi(0, y, t) &= \alpha_1, \quad \phi(L_1, y, t) = \alpha_2, \\ \phi(x, 0, t) &= \beta_1, \quad \phi(x, L_2, t) = \beta_2, \end{aligned} \quad (17)$$

in which the above partial differential equation is the scalar form of (1). Here $\phi = \phi(x, y, t)$ and $\mathbf{v} = (\bar{u}, \bar{v})$ is the advection velocity where \bar{u} and \bar{v} are the average velocity in x -direction and y -direction, respectively. In this section, we will analyze the convergence of the finite difference method with the implicit FTCS scheme applied to (17). Discretizing domain of the problem: $(x_i, y_j, t_n) \in \tilde{D}_h \times [0, T]_k$, where the spatial grid \tilde{D}_h is defined in (5) and the time grid $[0, T]_k$ has points t_n with $n \in K = \{0, 1, 2, \dots, N\}$.

According to Lax's equivalence theorem, we first show the consistency of the method. The implicit FTCS scheme of Eq. (17) is as follows

$$\begin{aligned} L_h \phi^h &\equiv \frac{\phi_{i,j}^{n+1} - \phi_{i,j}^n}{\Delta t} + \bar{u} \frac{\phi_{i+1,j}^{n+1} - \phi_{i-1,j}^{n+1}}{2\Delta x} + \bar{v} \frac{\phi_{i,j+1}^{n+1} - \phi_{i,j-1}^{n+1}}{2\Delta y} \\ &- \varepsilon \left[\frac{\phi_{i+1,j}^{n+1} - 2\phi_{i,j}^{n+1} + \phi_{i-1,j}^{n+1}}{(\Delta x)^2} + \frac{\phi_{i,j+1}^{n+1} - 2\phi_{i,j}^{n+1} + \phi_{i,j-1}^{n+1}}{(\Delta y)^2} \right] \\ &+ \kappa \phi_{i,j}^{n+1} = q_{i,j}^n. \end{aligned} \quad (18)$$

The truncation error for (17) obtained using the method is

$$\begin{aligned} T.E. &= \left(-\frac{\Delta t}{2!} \frac{\partial^2 \phi}{\partial t^2} - \frac{(\Delta t)^2}{3!} \frac{\partial^3 \phi}{\partial t^3} - \frac{(\Delta t)^3}{4!} \frac{\partial^4 \phi}{\partial t^4} - \dots \right) \\ &+ \bar{u} \left(-\frac{(\Delta x)^2}{3!} \frac{\partial^3 \phi}{\partial x^3} - \frac{(\Delta x)^4}{5!} \frac{\partial^5 \phi}{\partial x^5} - \frac{(\Delta x)^6}{7!} \frac{\partial^7 \phi}{\partial x^7} - \dots \right) \\ &+ \bar{v} \left(-\frac{(\Delta y)^2}{3!} \frac{\partial^3 \phi}{\partial y^3} - \frac{(\Delta y)^4}{5!} \frac{\partial^5 \phi}{\partial y^5} - \frac{(\Delta y)^6}{7!} \frac{\partial^7 \phi}{\partial y^7} - \dots \right) \\ &+ \varepsilon \left[\left(\frac{2(\Delta x)^2}{4!} \frac{\partial^4 \phi}{\partial x^4} + \frac{2(\Delta x)^4}{6!} \frac{\partial^6 \phi}{\partial x^6} + \frac{2(\Delta x)^6}{8!} \frac{\partial^8 \phi}{\partial x^8} + \dots \right) \right. \\ &\left. + \left(\frac{2(\Delta y)^2}{4!} \frac{\partial^4 \phi}{\partial y^4} + \frac{2(\Delta y)^4}{6!} \frac{\partial^6 \phi}{\partial y^6} + \frac{2(\Delta y)^6}{8!} \frac{\partial^8 \phi}{\partial y^8} + \dots \right) \right]. \end{aligned} \quad (19)$$

In other words, from (19), we have

$$T.E. = O((\Delta t), (\Delta x)^2, (\Delta y)^2).$$

Taking $(\Delta t, \Delta x, \Delta y) \rightarrow 0$, then we have

$$\begin{aligned} &\lim_{(\Delta t, \Delta x, \Delta y) \rightarrow 0} \|T.E.\| \\ &= \lim_{(\Delta t, \Delta x, \Delta y) \rightarrow 0} \|O((\Delta t), (\Delta x)^2, (\Delta y)^2)\| \\ &= 0 \end{aligned}$$

Secondly, we will demonstrate the stability of the finite difference method with the implicit FTCS scheme used to numerically solve (17). In consequence, the convergence of the proposed method will be obtained. In order to illustrate stability of the method, we initially show that condition (16) holds for the homogeneous equation of (17) and then condition (14) is satisfied for the nonhomogeneous equation (17). For convenience, we set $\tau = \Delta t$, $h = \Delta x = \Delta y$.

Case I: Homogeneous equation

Setting $q_{i,j}^n = 0$ in equation (18), scheme (18) becomes the discretized homogeneous version of (17). Assuming a discretized solution of the resulting equation as $\phi_{i,j}^n = \lambda^n e^{I(\alpha i + \beta j)}$, $I = \sqrt{-1}$, then the resulting homogeneous equation turns out to be

$$\begin{aligned} &\frac{\lambda^{n+1} e^{I(\alpha i + \beta j)} - \lambda^n e^{I(\alpha i + \beta j)}}{\tau} \\ &+ \bar{u} \frac{\lambda^{n+1} e^{I(\alpha(i+1) + \beta j)} - \lambda^{n+1} e^{I(\alpha(i-1) + \beta j)}}{2h} \\ &+ \bar{v} \frac{\lambda^{n+1} e^{I(\alpha i + \beta(j+1))} - \lambda^{n+1} e^{I(\alpha i + \beta(j-1))}}{2h} \\ &- \varepsilon \left[\frac{\lambda^{n+1} e^{I(\alpha(i+1) + \beta j)} - 2\lambda^{n+1} e^{I(\alpha i + \beta j)}}{h^2} \right. \\ &+ \frac{\lambda^{n+1} e^{I(\alpha(i-1) + \beta j)} + \lambda^{n+1} e^{I(\alpha i + \beta(j+1))}}{h^2} \\ &\left. + \frac{-2\lambda^{n+1} e^{I(\alpha i + \beta j)} + \lambda^{n+1} e^{I(\alpha i + \beta(j-1))}}{h^2} \right] \\ &+ \kappa \lambda^{n+1} e^{I(\alpha i + \beta j)} = 0. \end{aligned}$$

Algebraically manipulating the above equation, we have

$$\begin{aligned} \lambda^n e^{I(\alpha i + \beta j)} \left[\frac{\lambda - 1}{\tau} \right] - \lambda^{n+1} e^{I(\alpha i + \beta j)} \left[-\bar{u} \frac{e^{I\alpha} - e^{-I\alpha}}{2h} \right. \\ \left. - \bar{v} \frac{e^{I\beta} - e^{-I\beta}}{2h} + \varepsilon \frac{e^{I\alpha} - 2 + e^{-I\alpha}}{h^2} \right. \\ \left. + \varepsilon \frac{e^{I\beta} - 2 + e^{-I\beta}}{h^2} - \kappa \right] = 0, \end{aligned}$$

$$\begin{aligned} \left[\frac{\lambda - 1}{\tau} \right] - \frac{\lambda}{h} \left[-\bar{u} I \sin \alpha - \bar{v} I \sin \beta - \frac{4\varepsilon}{h} \sin^2 \frac{\alpha}{2} \right. \\ \left. - \frac{4\varepsilon}{h} \sin^2 \frac{\beta}{2} - \kappa h \right] = 0, \end{aligned}$$

$$\begin{aligned} [\lambda - 1] + \frac{\lambda \tau}{h} \left[\bar{u} I \sin \alpha + \bar{v} I \sin \beta + \frac{4\varepsilon}{h} \sin^2 \frac{\alpha}{2} \right. \\ \left. + \frac{4\varepsilon}{h} \sin^2 \frac{\beta}{2} + \kappa h \right] = 0, \end{aligned}$$

$$\begin{aligned} \lambda \left(1 + \frac{\tau}{h} \left[\bar{u} I \sin \alpha + \bar{v} I \sin \beta + \frac{4\varepsilon}{h} \sin^2 \frac{\alpha}{2} \right. \right. \\ \left. \left. + \frac{4\varepsilon}{h} \sin^2 \frac{\beta}{2} + \kappa h \right] \right) - 1 = 0, \end{aligned}$$

$$\lambda = \frac{1}{1 + \frac{\tau}{h} \left[\frac{4\varepsilon}{h} \left(\sin^2 \frac{\alpha}{2} + \sin^2 \frac{\beta}{2} \right) + I(\bar{u} \sin \alpha + \bar{v} \sin \beta) + \kappa h \right]},$$

Letting $\gamma = \frac{4\varepsilon\tau}{h^2}$ and $\eta = \frac{\tau}{h}$, we then obtain,

$$\lambda = \frac{1}{1 + \gamma \left(\sin^2 \frac{\alpha}{2} + \sin^2 \frac{\beta}{2} \right) + \eta I (\bar{u} \sin \alpha + \bar{v} \sin \beta) + \kappa\tau}$$

Consequently, the magnitude of λ is

$$|\lambda| = \frac{1}{\sqrt{[1 + \gamma \left(\sin^2 \frac{\alpha}{2} + \sin^2 \frac{\beta}{2} \right) + \kappa\tau]^2 + [\eta (\bar{u} \sin \alpha + \bar{v} \sin \beta)]^2}} \leq 1.$$

Therefore, the Von Neumann stability for the scheme, which is here independent of τ and h is obtained.

Case II: Nonhomogeneous equation

To show the sufficient condition for stability of the scheme. For sufficient condition $q(x, y, t) \neq 0$ we have to solve linear system of equation to find $\phi_{i,j}^{n+1}$ by known $\phi_{i,j}^n$

$$L_h \phi^h = \frac{\phi_{i,j}^{n+1} - \phi_{i,j}^n}{\tau} + \bar{u} \frac{\phi_{i+1,j}^{n+1} - \phi_{i-1,j}^{n+1}}{2h} + \bar{v} \frac{\phi_{i,j+1}^{n+1} - \phi_{i,j-1}^{n+1}}{2h} - \varepsilon \left[\frac{\phi_{i+1,j}^{n+1} - 2\phi_{i,j}^{n+1} + \phi_{i-1,j}^{n+1}}{h^2} + \frac{\phi_{i,j+1}^{n+1} - 2\phi_{i,j}^{n+1} + \phi_{i,j-1}^{n+1}}{h^2} \right] + \kappa \phi_{i,j}^{n+1} = q_{i,j}^n \quad (20)$$

boundary conditions: $\phi_{0,j}^n = \alpha_1, \phi_{N_1,j}^n = \alpha_2$
 $; j = 0, 1, \dots, N_2$
 $\phi_{i,0}^n = \beta_1, \phi_{i,N_2}^n = \beta_2$
 $; i = 0, 1, \dots, N_1.$ (21)

Rearrange, we get

$$a\phi_{i-1,j}^{n+1} + b\phi_{i,j-1}^{n+1} + c\phi_{i,j}^{n+1} + d\phi_{i+1,j}^{n+1} + e\phi_{i,j+1}^{n+1} = \varphi_{i,j}^n, \quad (22)$$

where

$$a = \left(\frac{\bar{u}\tau}{2h} + \frac{\varepsilon\tau}{h^2} \right), \quad b = \left(\frac{\bar{v}\tau}{2h} + \frac{\varepsilon\tau}{h^2} \right), \quad c = \left(-1 - \frac{4\varepsilon\tau}{h^2} - \kappa\tau \right),$$

$$d = \left(-\frac{\bar{u}\tau}{2h} + \frac{\varepsilon\tau}{h^2} \right), \quad e = \left(-\frac{\bar{v}\tau}{2h} + \frac{\varepsilon\tau}{h^2} \right), \quad \varphi_{i,j}^n = -\phi_{i,j}^n - \tau q_{i,j}^n.$$

The coefficients a, b, c, d, e satisfy the condition

$$a > 0, \quad b > 0, \quad d > 0, \quad e > 0, \quad |c| > a + b + d + e + \delta, \quad \delta > 0. \quad (23)$$

Lemma 3.1: If the coefficients of eq.(22) satisfy condition eq.(23) then solution of eq.(22) exist and unique and satisfy the inequality

$$|\phi_{i,j}^{n+1}| \leq \max \left\{ |\alpha_1|, |\alpha_2|, |\beta_1|, |\beta_2|, \frac{1}{\delta} \max_{r,s} |\varphi_{r,s}^n| \right\} \quad (24)$$

Proof: First, we proof inequality (24). Assume that $|\phi_{r,s}^{n+1}| = \max\{|\phi_{i,j}^{n+1}|, i = 0, 1, \dots, N_1, j = 0, 1, \dots, N_2\}$.

Let $0 < r < N_1, 0 < s < N_2$, then

$$\begin{aligned} |c||\phi_{r,s}^{n+1}| &= |-a\phi_{r-1,s}^{n+1} - b\phi_{r,s-1}^{n+1} - d\phi_{r+1,s}^{n+1} \\ &\quad - e\phi_{r,s+1}^{n+1} + \varphi_{r,s}^n| \\ &\leq |a\phi_{r-1,s}^{n+1}| + |b\phi_{r,s-1}^{n+1}| + |d\phi_{r+1,s}^{n+1}| \\ &\quad + |e\phi_{r,s+1}^{n+1}| + |\varphi_{r,s}^n| \\ &= |a||\phi_{r-1,s}^{n+1}| + |b||\phi_{r,s-1}^{n+1}| + |d||\phi_{r+1,s}^{n+1}| \\ &\quad + |e||\phi_{r,s+1}^{n+1}| + |\varphi_{r,s}^n| \\ &\leq (|a| + |b| + |d| + |e|)|\phi_{r,s}^{n+1}| + |\varphi_{r,s}^n| \\ |\phi_{r,s}^{n+1}| &\leq \frac{|\varphi_{r,s}^n|}{|c| - |a| - |b| - |d| - |e|} \\ &\leq \frac{|\varphi_{r,s}^n|}{\delta} \end{aligned}$$

This complete the proof. \square

Now we will prove the stability of the implicit FTCS scheme by showing that inequality (13) is satisfied. Let i^* and j^* be the smallest non-negative integers such that $(i^*, j^*) \in J$ and

$$|\phi_{i^*,j^*}^{n+1}| = \max_{(i,j) \in J} |\phi_{i,j}^{n+1}|, \quad (25)$$

where $J = \{(i, j) \mid i = 0, 1, 2, \dots, N_1, j = 0, 1, 2, \dots, N_2\}$. Denote $\bar{J} = \{(i, j) \in J \mid i = 0, N_1\} \cup \{(i, j) \in J \mid i \neq 0, N_1 \text{ and } j = 0, N_2\}$, i.e., \bar{J} is the discretized boundary set of J . It is obvious that if $(i^*, j^*) \in \bar{J}$, then we have

$$\max_{(i,j) \in J} |\phi_{i,j}^{n+1}| \leq \max\{|\alpha_1|, |\alpha_2|, |\beta_1|, |\beta_2|\}. \quad (26)$$

If $(i^*, j^*) \in \mathcal{I} = J - \bar{J}$, then replacing (i, j) in (20) with (i^*, j^*) we obtain

$$\begin{aligned} &\left(\frac{\bar{u}\tau}{2h} + \frac{\varepsilon\tau}{h^2} \right) \phi_{i^*-1,j^*}^{n+1} + \left(\frac{\bar{v}\tau}{2h} + \frac{\varepsilon\tau}{h^2} \right) \phi_{i^*,j^*-1}^{n+1} \\ &- \left(1 + \frac{4\varepsilon\tau}{h^2} + \kappa\tau \right) \phi_{i^*,j^*}^{n+1} - \left(\frac{\bar{u}\tau}{2h} - \frac{\varepsilon\tau}{h^2} \right) \phi_{i^*+1,j^*}^{n+1} \\ &- \left(\frac{\bar{v}\tau}{2h} - \frac{\varepsilon\tau}{h^2} \right) \phi_{i^*,j^*+1}^{n+1} = -\phi_{i^*,j^*}^n - \tau q_{i^*,j^*}^n. \end{aligned} \quad (27)$$

Next we announce the following hypothesis:

$$\text{(H1)} : \begin{aligned} \bar{u} [\phi_{i^*-1,j^*}^{n+1} - \phi_{i^*+1,j^*}^{n+1}] &\leq 0, \\ \bar{v} [\phi_{i^*,j^*-1}^{n+1} - \phi_{i^*,j^*+1}^{n+1}] &\leq 0. \end{aligned} \quad (28)$$

Without loss of generality we assume that $\phi_{i^*,j^*}^{n+1} > 0$ and further assume that the hypothesis (H1) holds. We can estimate the left side of (27) as

$$\begin{aligned} &\frac{\varepsilon\tau}{h^2} [\phi_{i^*-1,j^*}^{n+1} - \phi_{i^*,j^*}^{n+1}] + \frac{\varepsilon\tau}{h^2} [\phi_{i^*,j^*-1}^{n+1} - \phi_{i^*,j^*}^{n+1}] \\ &+ \frac{\varepsilon\tau}{h^2} [\phi_{i^*+1,j^*}^{n+1} - \phi_{i^*,j^*}^{n+1}] + \frac{\varepsilon\tau}{h^2} [\phi_{i^*,j^*+1}^{n+1} - \phi_{i^*,j^*}^{n+1}] \\ &+ \frac{\tau\bar{u}}{2h} [\phi_{i^*-1,j^*}^{n+1} - \phi_{i^*+1,j^*}^{n+1}] + \frac{\tau\bar{v}}{2h} [\phi_{i^*,j^*-1}^{n+1} - \phi_{i^*,j^*+1}^{n+1}] \\ &- \phi_{i^*,j^*}^{n+1} - \kappa\tau\phi_{i^*,j^*}^{n+1} \\ &\leq -\phi_{i^*,j^*}^{n+1}. \end{aligned} \quad (29)$$

We then obtain

$$\phi_{i^*,j^*}^{n+1} \leq \phi_{i^*,j^*}^n + \tau q_{i^*,j^*}^n, \quad (30)$$

and we consequently have,

$$\begin{aligned} \max_{(i,j) \in J} |\phi_{i,j}^{n+1}| &\leq \max_{(i,j) \in J} |\phi_{i,j}^n + \tau q_{i,j}^n| \\ &\leq \max_{(i,j) \in J} |\phi_{i,j}^n| + \tau \max_{\substack{(i,j) \in J \\ n \in K}} |q_{i,j}^n|, \end{aligned} \quad (31)$$

where $K = \{0, 1, 2, \dots, N\}$. We now establish the following inequality representing the maximum principle as

$$\max_{(i,j) \in J} |\phi_{i,j}^{n+1}| \leq \max \left\{ |\alpha_1|, |\alpha_2|, |\beta_1|, |\beta_2|, \max_{(i,j) \in J} |\phi_{i,j}^n| + \tau \max_{\substack{(i,j) \in J \\ n \in K}} |q_{i,j}^n| \right\}. \quad (32)$$

Separating the discretized solution ϕ^h of (18) into

$$\phi^h = v^h + w^h, \quad (33)$$

where v^h and w^h satisfy the equations

$$L_h v^h = \begin{cases} 0 \\ \psi_0(x_i, y_j) \\ \alpha_1 \\ \alpha_2 \\ \beta_1 \\ \beta_2 \end{cases}, \quad L_h w^h = \begin{cases} q(x_i, y_j, t_n) \\ 0 \\ 0 \\ 0 \\ 0 \\ 0 \end{cases}, \quad (34)$$

we use (32) to find a bound of each problem in (34) as follows. Firstly applying (32) to the first problem of (34), we have

$$\max_{(i,j) \in J} |v_{i,j}^{n+1}| \leq \max \left\{ |\alpha_1|, |\alpha_2|, |\beta_1|, |\beta_2|, \max_{(i,j) \in J} |v_{i,j}^n| \right\} \quad (35)$$

for $n = 0, 1, 2, \dots, N-1$. Relabelling the superscript indices of v^h in (35), we have the following inequalities:

$$\begin{aligned} \max_{(i,j) \in J} |v_{i,j}^n| &\leq \max \left\{ |\alpha_1|, |\alpha_2|, |\beta_1|, |\beta_2|, \max_{(i,j) \in J} |v_{i,j}^{n-1}| \right\} \\ \max_{(i,j) \in J} |v_{i,j}^{n-1}| &\leq \max \left\{ |\alpha_1|, |\alpha_2|, |\beta_1|, |\beta_2|, \max_{(i,j) \in J} |v_{i,j}^{n-2}| \right\} \\ &\vdots \\ \max_{(i,j) \in J} |v_{i,j}^1| &\leq \max \left\{ |\alpha_1|, |\alpha_2|, |\beta_1|, |\beta_2|, \max_{(i,j) \in J} |\psi_{i,j}^0| \right\}. \end{aligned}$$

Therefore, we obtain

$$\max_{(i,j) \in J} |v_{i,j}^{n+1}| \leq \max \left\{ |\alpha_1|, |\alpha_2|, |\beta_1|, |\beta_2|, \max_{(i,j) \in J} |\psi_{i,j}^0| \right\}. \quad (36)$$

Secondly applying (32) n times to the last problem of (34), we obtain

$$\begin{aligned} \max_{(i,j) \in J} |w_{i,j}^{n+1}| &\leq \max_{(i,j) \in J} |w_{i,j}^n| + \tau \max_{\substack{(i,j) \in J \\ n \in K}} |q_{i,j}^n| \\ &\leq \max_{(i,j) \in J} |w_{i,j}^{n-1}| + 2\tau \max_{\substack{(i,j) \in J \\ n \in K}} |q_{i,j}^n| \\ &\vdots \\ &\leq \max_{(i,j) \in J} |w_{i,j}^0| + (n+1)\tau \max_{\substack{(i,j) \in J \\ n \in K}} |q_{i,j}^n| \\ &\leq (N+1)\tau \max_{\substack{(i,j) \in J \\ n \in K}} |q_{i,j}^n| \\ &\leq 2T \max_{\substack{(i,j) \in J \\ n \in K}} |q_{i,j}^n|. \end{aligned}$$

Thus, we have that

$$\max_{(i,j) \in J} |w_{i,j}^{n+1}| \leq 2T \max_{\substack{(i,j) \in J \\ n \in K}} |q_{i,j}^n|. \quad (37)$$

Using both inequalities (36) and (37), we finally obtain

$$\begin{aligned} \max_{(i,j) \in J} |\phi_{i,j}^{n+1}| &= \max_{(i,j) \in J} |v_{i,j}^{n+1} + w_{i,j}^{n+1}| \\ &\leq \max_{(i,j) \in J} |v_{i,j}^{n+1}| + \max_{(i,j) \in J} |w_{i,j}^{n+1}| \\ &\leq \max \left\{ |\alpha_1|, |\alpha_2|, |\beta_1|, |\beta_2|, \max_{(i,j) \in J} |\psi_{i,j}^0| \right\} \\ &\quad + 2T \max_{\substack{(i,j) \in J \\ n \in K}} |q_{i,j}^n|. \\ &\leq \|f^h\|_{H_h} + 2T \|f^h\|_{H_h} \\ &= C \|f^h\|_{H_h}, \end{aligned} \quad (38)$$

where $C = (1 + 2T)$. The above inequality is true for any n , we hence have that

$$\|\phi^h\|_{\Omega_h} \leq C \|f^h\|_{H_h}, \quad (39)$$

where

$$\|\phi^h\|_{\Omega_h} = \max_{\substack{(i,j) \in J \\ n \in K}} |\phi_{i,j}^n| \quad (40)$$

$$\|f^h\|_{H_h} = \max \left(|\alpha_1|, |\alpha_2|, |\beta_1|, |\beta_2|, \max_{\substack{(i,j) \in J \\ n \in K}} |q_{i,j}^n| \right).$$

IV. VALIDATION

To validate the present numerical scheme, the one-dimensional advection-diffusion equation [26]–[28]

$$\frac{\partial C}{\partial t} + \bar{u} \frac{\partial C}{\partial x} - D_f \frac{\partial^2 C}{\partial x^2} = 0, \quad 0 \leq x \leq 1, \quad 0 < t \leq 1 \quad (41)$$

is used as the test case. Eq. (41) can be utilized to measure the pollutant concentration $C(x, t)$ in a flow stream. The variable and parameters in (41) are described as follows: x is the longitudinal distance along the stream, t is time, $C(x, t)$ is the concentration (kg/m^3) averaged in depth at the point x and at time t , \bar{u} is the water flow velocity in the x -direction, and D_f is the dispersion coefficient. It is found from [26]–[28] that if $\bar{u} = 1$ and $D_f = 0.01$ then the analytical solution of (41) is

$$C(x, t) = \frac{0.025}{\sqrt{0.000625 + 0.02t}} \exp \left[-\frac{(x + 0.5 - t)^2}{(0.00125 + 0.04t)} \right], \quad (42)$$

provided that the initial condition is

$$C(x, 0) = e^{-800(x+0.5)^2}, \quad 0 < x < 1, \quad (43)$$

and the boundary conditions are

$$C(0, t) = \frac{0.025}{\sqrt{0.000625 + 0.02t}} \exp \left[-\frac{(0.5 - t)^2}{(0.00125 + 0.04t)} \right], \quad 0 < t < 1, \quad (44)$$

$$C(1, t) = \frac{0.025}{\sqrt{0.000625 + 0.02t}} \exp \left[-\frac{(1.5 - t)^2}{(0.00125 + 0.04t)} \right], \quad 0 < t < 1. \quad (45)$$

The 3D graph of the analytical solution (42) of the initial-boundary value problem consisting of (41) and (43)–(45) is plotted on the domain as shown in Fig. 1.

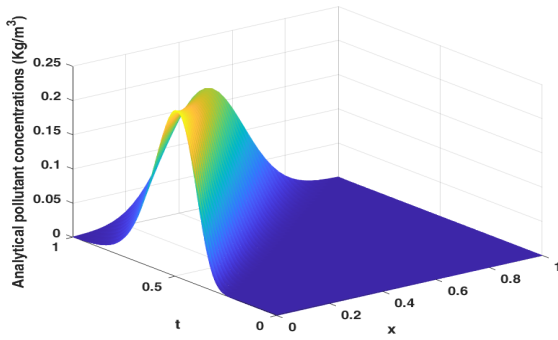


Fig. 1. The 3D graph of the analytical solution $C(x, t)$ of the initial-boundary value problem consisting of (41) and (43)-(45).

The implicit FTCS scheme applied to the above problem for obtaining the approximated pollutant concentration $C(x, t)$ is given as

$$\frac{\phi_{i,j}^{n+1} - \phi_{i,j}^n}{\Delta t} + \bar{u} \frac{\phi_{i+1,j}^{n+1} - \phi_{i-1,j}^{n+1}}{2\Delta x} - D_f \left(\frac{\phi_{i+1,j}^{n+1} - 2\phi_{i,j}^{n+1} + \phi_{i-1,j}^{n+1}}{\Delta x^2} \right) = 0. \quad (46)$$

Substituting $\Delta x = 0.0250$, $\Delta t = 0.0020$ and the conditions (43)-(45) into the above scheme, we obtain the numerical water pollutant concentration $C(x, t)$ on the discretized domain as demonstrated in Fig.2. Two comparisons between the analytical and numerical pollutant concentrations are investigated by fixing $t = 1$ and $x = 0.5$. Firstly, the analytical and numerical solutions of the problem when $t = 1$ and $0 \leq x \leq 1$ are depicted in Fig.3. It is noticed that the maximum values of the water pollutant concentration obtained by the analytical and numerical solutions occur at $x \approx 0.5$. In addition, the scheme numerically gives the maximum absolute error of 5.3×10^{-3} when compared with the analytical solution at $x \approx 0.5$. Secondly, Fig.4 show the comparison between analytical and numerical pollutant concentrations of the test problem when x is fixed at $x = 0.5$ and $0 \leq t \leq 1$. We can observe that both solutions provide the maximum values of the water pollutant concentration at the final time $t = 1$. The maximum absolute error obtained using the method for this problem is approximately 5.7×10^{-3} when compared with the analytical solution on the discretized grid. Therefore, the proposed scheme is appropriate and trustworthy for computing numerical solutions of the real-world problem because it is a straightforward method and not difficult to write computer-codes.

V. NUMERICAL RESULTS

Applications of the ADRE to construct a governing equation for water pollution problems have been found in [28]–[33]. In this section, we will use the implicit FTCS scheme to numerically solve the water pollution problem which can be formulated using the ADRE. The considering problem consists of a two-dimensional advection-diffusion-reaction equation, initial and boundary conditions. The two-dimensional ADRE representing the model dispersion of a water pollutant with non-removal and removal mechanism is expressed as [33]:

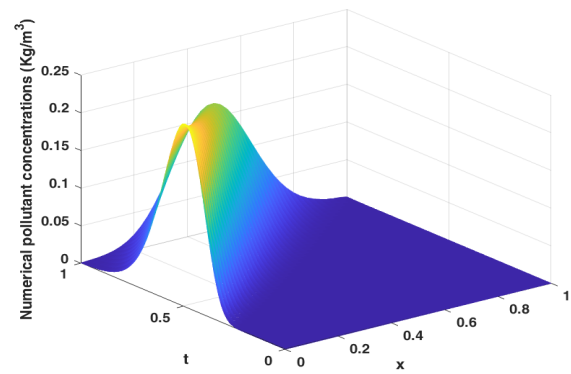


Fig. 2. The 3D graph of the numerical solution $C(x, t)$ of the initial-boundary value problem consisting of (41) and (43)-(45) using the implicit FTCS scheme with $\Delta x = 0.0250$, $\Delta t = 0.0020$.

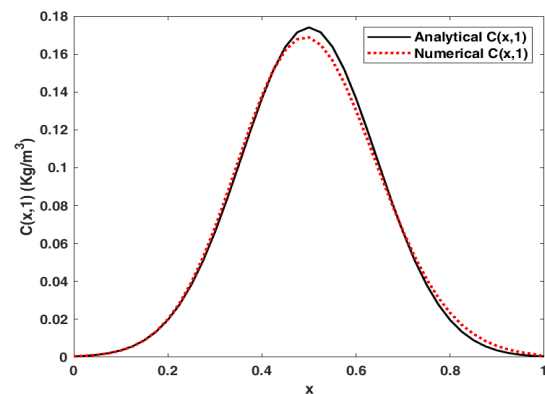


Fig. 3. Comparison between the analytical solution and numerical solution ($\Delta x = 0.0250$, $\Delta t = 0.0020$) for the test problem using $t = 1$ and $0 \leq x \leq 1$.

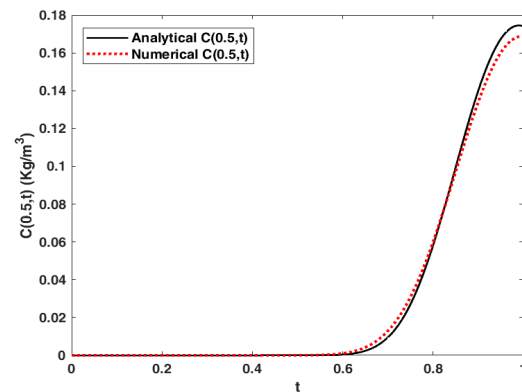


Fig. 4. Comparison between the analytical solution and numerical solution ($\Delta x = 0.0250$, $\Delta t = 0.0020$) for the test problem using $x = 0.5$ and $0 \leq t \leq 1$.

$$\frac{\partial C}{\partial t} + \bar{u} \frac{\partial C}{\partial x} + \bar{v} \frac{\partial C}{\partial y} - D_f \left(\frac{\partial^2 C}{\partial x^2} + \frac{\partial^2 C}{\partial y^2} \right) + RC = Q(x, y, t), \quad (47)$$

where $C(x, y, t)$ is the water pollutant concentration averaged in depth at the point $\mathbf{x} = (x, y)$ at time t (kg/m^3), \bar{u} and \bar{v} are velocity components (m/s) in x - and y -directions, respectively, D_f is the pollutant dispersion coefficient (m^2/s),

$R \geq 0$ is the decay rate of water pollutant (s^{-1}), and $Q(x, y, t)$ is a decreasing rate of water pollutant concentration due to a water pollutant sink (kg/m^3s). The initial pollutant concentration in reservoir is $C(x, y, 0) = c_0$ (kg/m^3). Since we want to study effects of the number of the entrance gates on $C(x, y, t)$, then we supply one and two entrance gates as our boundary conditions. The water pollutant is released from the open entrance gate into the reservoir, which is the averaged pollutant concentration along the entrance gate defined by c_1 (kg/m^3), where c_1 is a positive constant. The reservoir has drained water through the exit gate by assuming rate of water drain as $\partial C/\partial x = -c_2$ (kg/m^3), where c_2 is a non-negative constant. There is no rate of change of pollutant concentration at the boundary of the opened reservoir, $\partial C/\partial n = 0$, where n is a normal vector. The opened reservoirs equipped with the above initial and boundary conditions for one and two entrance gates are described by the diagrams in Fig. 5 and Fig. 6, respectively. Here our numerical experiments are calculated using three types of the decreasing rate of water pollutant concentration $Q(x, y, t)$ as follows:

- (a) $Q(x, y, t) = 0$,
- (b) $Q(x, y, t) = -0.01$,
- (c) $Q(x, y, t) = -e^{-t}$,

and the following parameter values [33]: the approximate velocity in x -direction is $\bar{u} = -0.002461$ and y -direction is $\bar{v} = 0.04527$ and the decaying rate $R = 0.1 \times 10^{-6}$. Also the following fixed initial and boundary conditions [33] $c_0 = 1.5$, $c_1 = 10$, $c_2 = 0.001$ are used in our simulations. However, the pollutant dispersion coefficient D_f is chosen as $D_f = 50, 100, 150, 200$ in our experiments. Defining the domain for (47) as $0 m \leq x, y \leq 2000 m$ and $0 s \leq t \leq 100 s$ and the spatial step size $\Delta x = \Delta y = 31.25 m$ and the time step size $\Delta t = 1 s$, the proposed scheme provides numerical solutions of the problems depending upon the number of the entrance gates as follows.

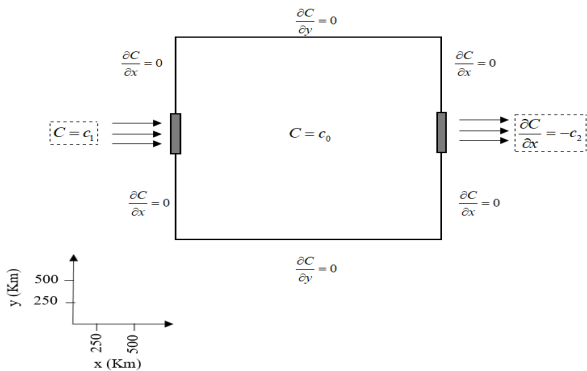


Fig. 5. The initial and boundary conditions of water pollutant dispersion model in the opened reservoir for one entrance gate.

A. Numerical solutions for one entrance gate reservoir

As mentioned, numerical simulations for this case are computed using three different cases of $Q(x, y, t)$, the initial condition and the boundary conditions as shown in Fig. 5. In each case, the coefficient $D_f = 50, 100, 150, 200$ are varied to perform the simulations. We consequently have the following results in which all of the graphs are plotted at the final time $t = 100 s$.

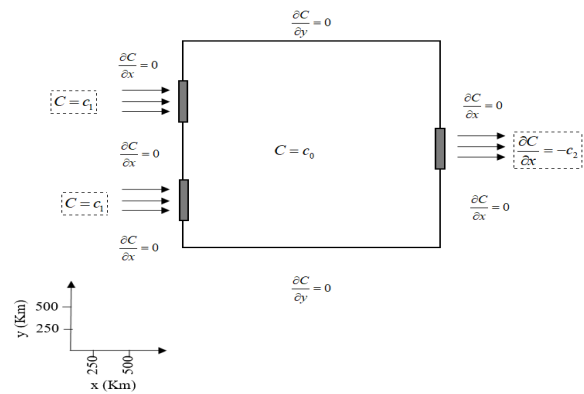


Fig. 6. The initial and boundary conditions of water pollutant dispersion model in the opened reservoir for two entrance gates.

(a) $Q(x, y, t) = 0$: The distributions of pollutant concentration $C(x, y, t)$ and their contours are depicted in Fig. 7 (a)-(d) and Fig. 8 (a)-(d), respectively when the coefficient D_f is varied as $D_f = 50, 100, 150, 200$. We can observe from these figures that the minimum value of $C(x, y, t)$ is about 1.5 (kg/m^3) and it decreases to $1.46, 1.41, 1.39, 1.38$ nearby the exit gate, respectively.

(b) $Q(x, y, t) = -0.01$: The distributions of pollutant concentration $C(x, y, t)$ and their contours are plotted in Fig. 9 (a)-(d) and Fig. 10 (a)-(d), respectively when the coefficient D_f is changed as $D_f = 50, 100, 150, 200$. It is noticed from these figures that the minimum value of $C(x, y, t)$ is about 0.5 (kg/m^3) and it is decreased as $0.44, 0.41, 0.39, 0.38$ (kg/m^3) nearby the exit gate, respectively.

(c) $Q(x, y, t) = -e^{-t}$: We have the distributions of pollutant concentration $C(x, y, t)$ and their contours as shown in Fig. 11 (a)-(d) and Fig. 12 (a)-(d), respectively when $D_f = 50, 100, 150, 200$. The minimum value of $C(x, y, t)$ is about 0.92 (kg/m^3) and it is decreased as $0.854, 0.852, 0.81, 0.79$ when close to the exit gate, respectively.

In addition, we attempt to observe the behaviors of the pollutant concentration at $y = 1000$, i.e., $C(x, 1000, t)$ for $0 m \leq x \leq 2000 m$ and $0 s \leq t \leq 100 s$. The distribution graphs of $C(x, 1000, t)$ when D_f fixed at 50 for $Q(x, y, t) = 0, -0.01$ and $-e^{-t}$ are shown in Fig. 13 (a)-(c), respectively. While the graphs of $C(x, 1000, t)$ when $D_f = 200$ for $Q(x, y, t) = 0, -0.01$ and $-e^{-t}$ are shown in Fig. 14 (a)-(c), respectively. We can see that $C(x, 1000, t)$ rapidly decreases as x and t initially increase and then the values $C(x, 1000, t)$ slightly change when x and t are sufficiently large. Furthermore, in case of $D_f = 50$, the values of $C(2000, 1000, 100)$ for $Q(x, y, t) = 0, -0.01$ and $-e^{-t}$ are $1.405, 0.405, 0.823$, respectively. For $D_f = 200$, the values of $C(2000, 1000, 100)$ for $Q(x, y, t) = 0, -0.01$ and $-e^{-t}$ are $1.345, 0.345, 0.763$, respectively. In particular, the pollutant concentration at $y = 1000$ when x nearby the entrance gate are plotted in Figs. 15-18 as follows. The 2D graphs of $C(125, 1000, t)$ for $D_f = 50$ and $D_f = 200$ are depicted in Fig. 15 and Fig. 17, respectively. It can be observed from these figures that the higher value of D_f results the higher value of $C(125, 1000, t)$ as t increases. Moreover, the higher value of D_f makes the x -intersection between the curves $C(125, 1000, t)$ for $Q(x, y, t) = -0.01$ and $Q(x, y, t) = -e^{-t}$ shorter. Furthermore, the 2D graphs

of $C(250, 1000, t)$ for $D_f = 50$ and $D_f = 200$ are portrayed in Fig. 16 and Fig. 18, respectively. The behaviors of these graphs are similar to Fig. 15 and Fig. 17. From all numerical results as described above, we can observe that the value of D_f slightly affects on $C(x, y, t)$, in other words, higher value of D_f makes the values of $C(x, y, t)$ a bit lower.

B. Numerical solutions for two entrance gates reservoir

The functions $Q(x, y, t)$, the initial condition, the boundary conditions and the pollutant dispersion coefficient D_f used for the previous case will be also utilized to obtain numerical simulations for the case of two entrance gates reservoir. The diagram of the reservoir for this case is drawn in Fig. 6. The numerical results for $t = 100$ s obtained using the the proposed scheme with the conditions and parameters as mentioned above are as follows.

(a) $Q(x, y, t) = 0$: The distributions of pollutant concentration $C(x, y, t)$ and their contours are depicted in Fig. 19 (a)-(d) and Fig. 20 (a)-(d), respectively when the coefficient D_f is varied as $D_f = 50, 100, 150, 200$. Since the two entrance gates are symmetric, then the numerical results are symmetrically similar about $y = 1000$ m. We can observe from these figures that the minimum value of $C(x, y, t)$ is around 1.5 (kg/m^3) and it decreases to $1.44, 1.41, 1.39, 1.38$ (kg/m^3) close to the exit gate, respectively.

(b) $Q(x, y, t) = -0.01$: The distributions of pollutant concentration $C(x, y, t)$ are plotted in Fig. 21 (a)-(d) when the coefficient D_f is changed as $D_f = 50, 100, 150, 200$, respectively. In addition, their contours are shown Fig. 22 (a)-(d). Because there are two entrance gates which are symmetric about $y = 1000$ m, then the numerical results around both gates are symmetrically similar. From these figures, the minimum value of $C(x, y, t)$ is about 0.5 (kg/m^3) and it is decreased to $0.44, 0.41, 0.39, 0.38$ nearby the exit gate, respectively.

(c) $Q(x, y, t) = -e^{-t}$: We have the distributions of pollutant concentration $C(x, y, t)$ in Fig. 23 (a)-(d) when $D_f = 50, 100, 150, 200$, respectively. The contours of $C(x, y, t)$ as shown Fig. 24 (a)-(d). The minimum value of $C(x, y, t)$ is about 0.92 (kg/m^3) and it is decreased to $0.85, 0.83, 0.81, 0.79$ when close to the exit gate, respectively. The symmetrical results of $C(x, y, t)$ occur about in the middle of y -axis.

From the contour plots in Figs. 20 (a)-(d), 22 (a)-(d) and 24 (a)-(d), we can observe that as the coefficient D_f is higher, the contours are more symmetric about $y = 1000$ m. For the case of two entrance gates, the numerical solutions for the first half part of y -axis are closely similar to the obtained results for the other half part.

Furthermore, we attempt to observe the behaviors of the pollutant concentration at $y = 500$ m and $y = 1000$ m for $0 \text{ m} \leq x \leq 2000 \text{ m}$ and $0 \text{ s} \leq t \leq 100 \text{ s}$ when D_f fixed only at 200 . The distribution graphs of $C(x, 500, t)$ and $C(x, 1000, t)$ for $Q(x, y, t) = 0, -0.01$ and $-e^{-t}$ are shown in Fig. 25 (a)-(c) and Fig. 26 (a)-(c), respectively. We can see that $C(x, 500, t)$ sharply decreases as x and t initially increase and then the values $C(x, 500, t)$ slightly change when x and t are adequately large. However, the behavior of $C(x, 1000, t)$ is different from the previous one. As a result, rapid reduction of $C(x, 1000, t)$ cannot be observed as x

and t initially increase. In particular, Fig. 26 (a) shows that there are some changes for $C(x, 1000, t)$, i.e., decreasing, maintaining constant, and decreasing when x moves from 0 to 2000 . In Fig. 26 (b), $C(x, 1000, t)$ behaves like a slant plane and decreases when x and t increase. Fig. 26 (c) shows that $C(x, 1000, t)$ has a sharp reduction for an initial amount of time and then its graph is quite flat as x and t increase. Moreover, the values of $C(2000, 500, 100)$ for $Q(x, y, t) = 0, -0.01$ and $-e^{-t}$ are $1.499, 0.499, 0.917$, respectively and the values of $C(2000, 1000, 100)$ for $Q(x, y, t) = 0, -0.01$ and $-e^{-t}$ are $1.345, 0.345, 0.763$, respectively. Particularly, the pollutant concentration at $y = 500$ and $y = 1000$ when x nearby the entrance gates, $Q(x, y, t) = 0, -0.01$ and $-e^{-t}$ and $D_f = 200$ are plotted in Figs. 27-30 as follows. The 2D graphs of $C(125, 500, t)$ are depicted in Fig. 27. It can be observed from these figures that the curves of $C(125, 500, t)$ tend to increase as t increases. The 2D graphs of $C(125, 1000, t)$ are plotted in Fig. 29. The curve of $C(125, 1000, t)$ for $Q(x, y, t) = 0$ seems to be quite constant for all values of t . For $Q(x, y, t) = -0.01$, the graph of $C(125, 1000, t)$ keeps decreasing as t increases. The graph of $C(125, 1000, t)$ for $Q(x, y, t) = -e^{-t}$ rapidly decreases in the first 5 second and then keep constantly as t increases. The 2D graphs of $C(250, 500, t)$ and $C(250, 1000, t)$ with $D_f = 200$ are also portrayed in Fig. 28 and Fig. 30, respectively. The behaviors of these graphs are similar to Fig. 27 and Fig. 29. From all numerical results, it can be concluded that at $y = 500$ m the behaviors of $C(x, 500, t)$ are similar for all $Q(x, y, t)$ but the behaviors of $C(x, 1000, t)$ are different at $y = 1000$ m depending on $Q(x, y, t)$.

VI. CONCLUSION

The convergence of finite difference method with the implicit forward time central space (FTCS) scheme applied to the 2-D advection-diffusion-reaction equation (ADRE) with the average velocity in x - and y -directions have been investigated via its consistency and stability. In other words, the truncation error from the scheme approaches zero when the grid sizes tend to zero. The scheme is unconditional stable when applied to the homogeneous ADRE and the criteria (14) is satisfied for the nonhomogeneous problem by establishing some conditions. In addition, the scheme has been applied to numerically solve the real problem of the ADRE which is the water pollution problem in the reservoir with one and two entrance gates. The decreasing rate of water pollutant concentration due to a water pollutant sink denoted by $Q(x, y, t)$ and the pollutant dispersion coefficient D_f are the parameters varied in the numerical simulations. In average, the water pollutant concentration $C(x, y, t)$ for $Q = -0.01$ and $Q = -e^{-t}$ is less than its concentration for $Q = 0$. In consequence, the water quality for the case $Q \neq 0$ is better than the quality of the case $Q = 0$. The value of $C(x, y, t)$ is quite high when close to the entrance gates but rapidly decreases when far away from the entrance gates. The numerical results have shown that the pollutant concentration in water can be distributed more when the dispersion coefficient (D_f) is higher.

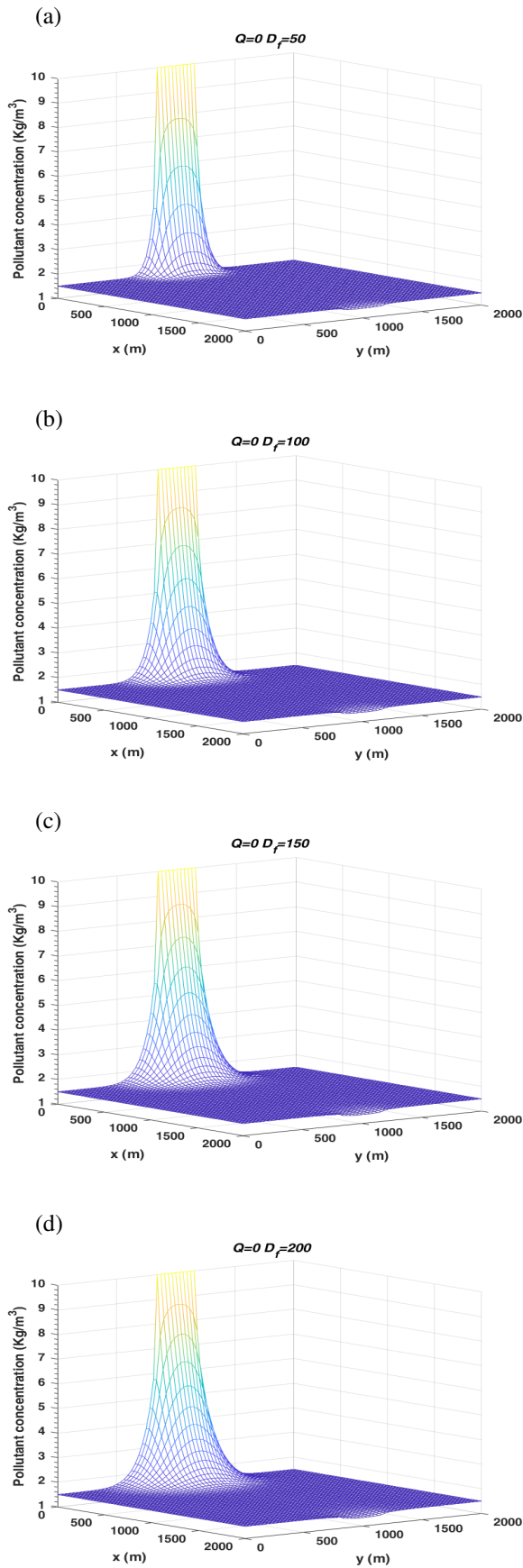


Fig. 7. The 3D graphs of the approximated pollutant concentrations for one entrance gate when $Q = 0$ and (a) $D_f = 50$, (b) $D_f = 100$, (c) $D_f = 150$ and (d) $D_f = 200$.

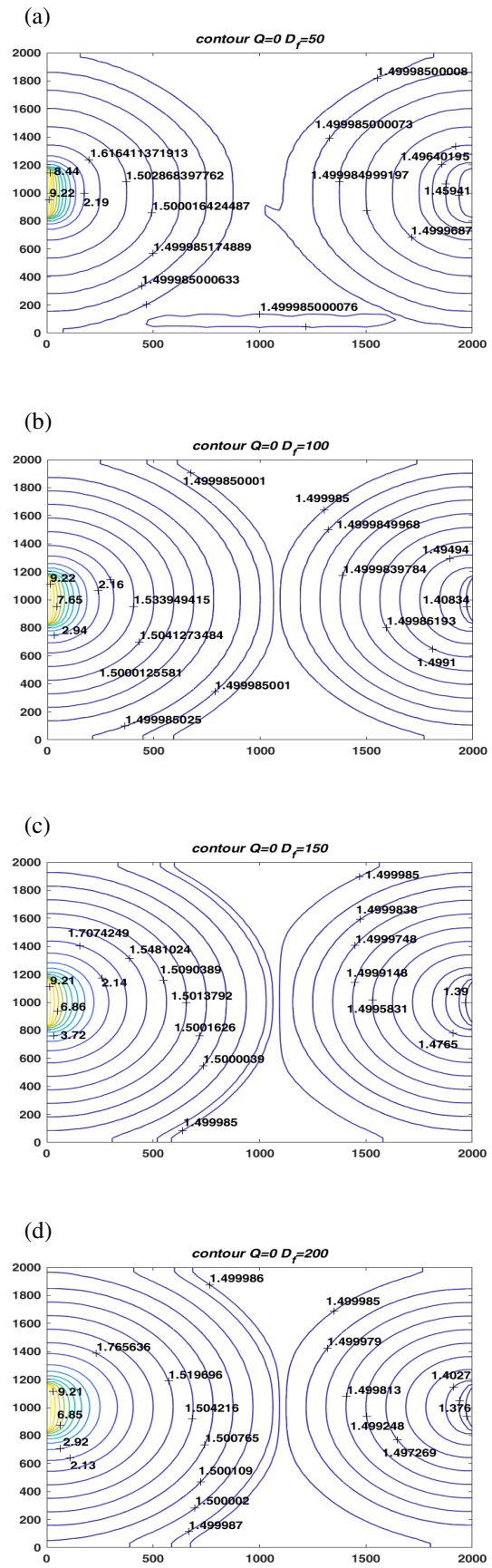


Fig. 8. The contour plots for one entrance gate case when $Q = 0$ and (a) $D_f = 50$, (b) $D_f = 100$, (c) $D_f = 150$ and (d) $D_f = 200$.

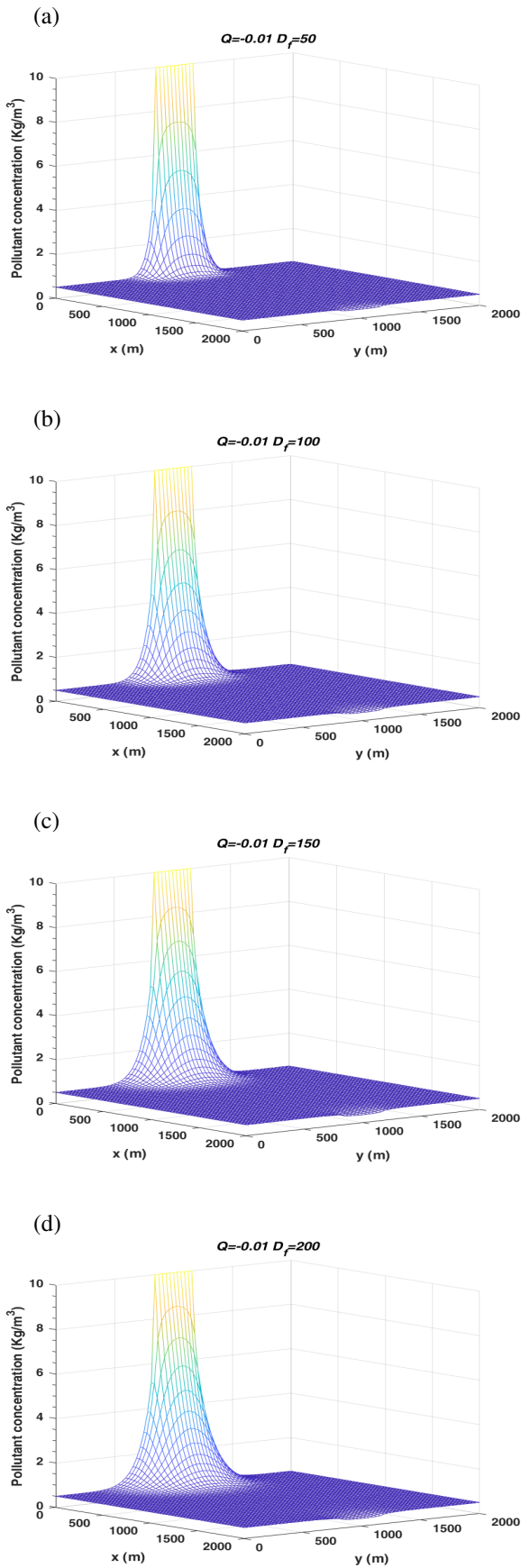


Fig. 9. The 3D graph of the approximated pollutant concentrations for one entrance gate case when $Q = -0.01$ and (a) $D_f = 50$, (b) $D_f = 100$, (c) $D_f = 150$ and (d) $D_f = 200$.

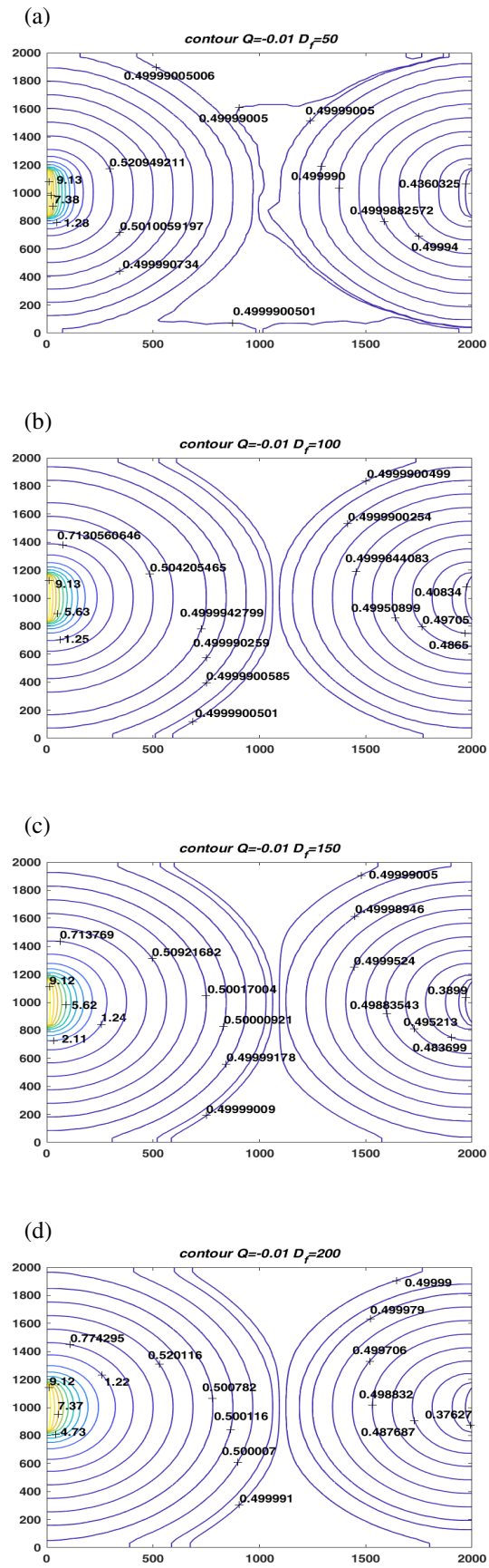


Fig. 10. The contour plots for one entrance gate case when $Q = -0.01$ and (a) $D_f = 50$, (b) $D_f = 100$, (c) $D_f = 150$ and (d) $D_f = 200$.

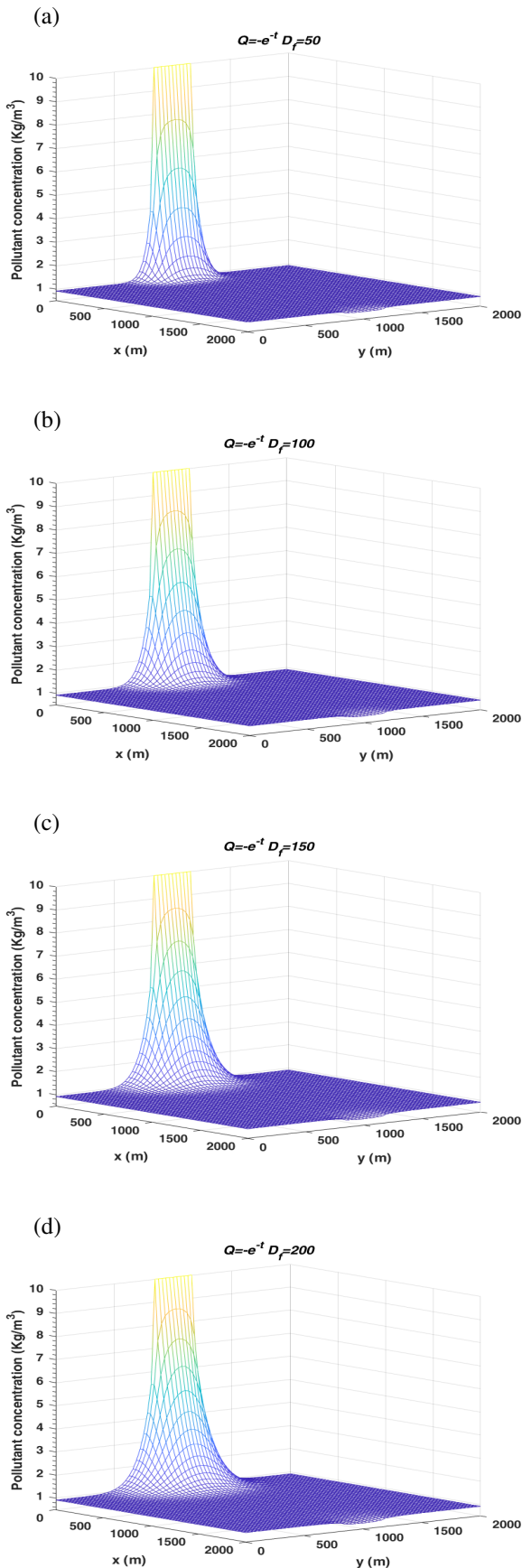


Fig. 11. The 3D graph of the approximated pollutant concentrations for one entrance gate case when $Q = -e^{-t}$ and (a) $D_f = 50$, (b) $D_f = 100$, (c) $D_f = 150$ and (d) $D_f = 200$.

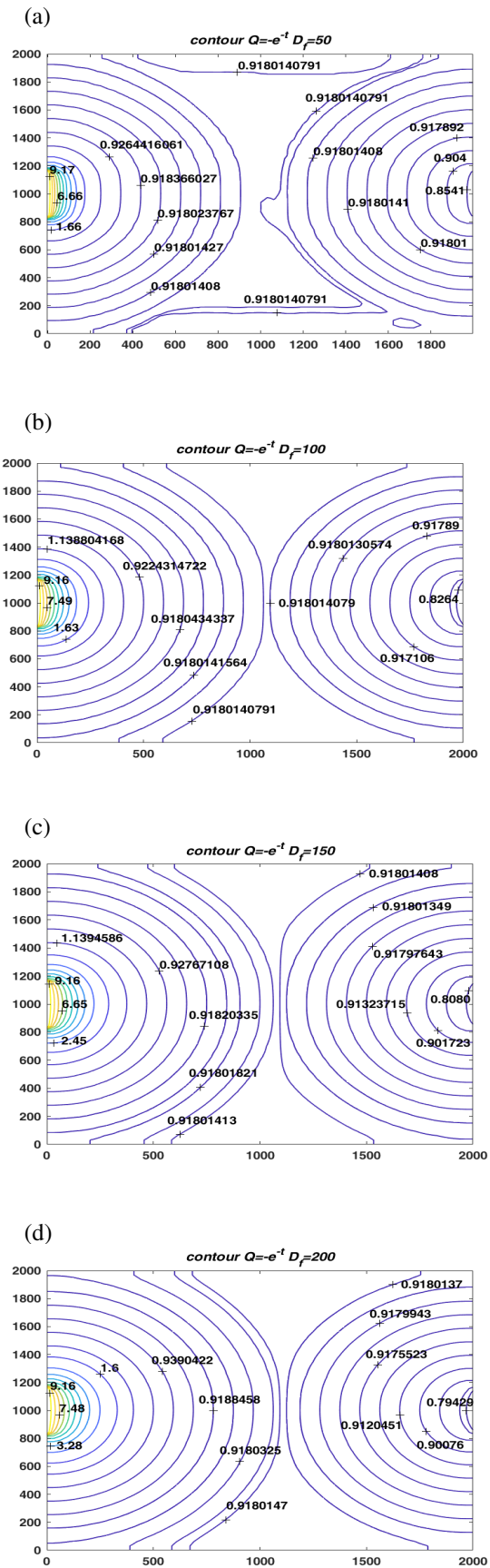


Fig. 12. The contour plots for one entrance gate case when $Q = -e^{-t}$ and (a) $D_f = 50$, (b) $D_f = 100$, (c) $D_f = 150$ and (d) $D_f = 200$.

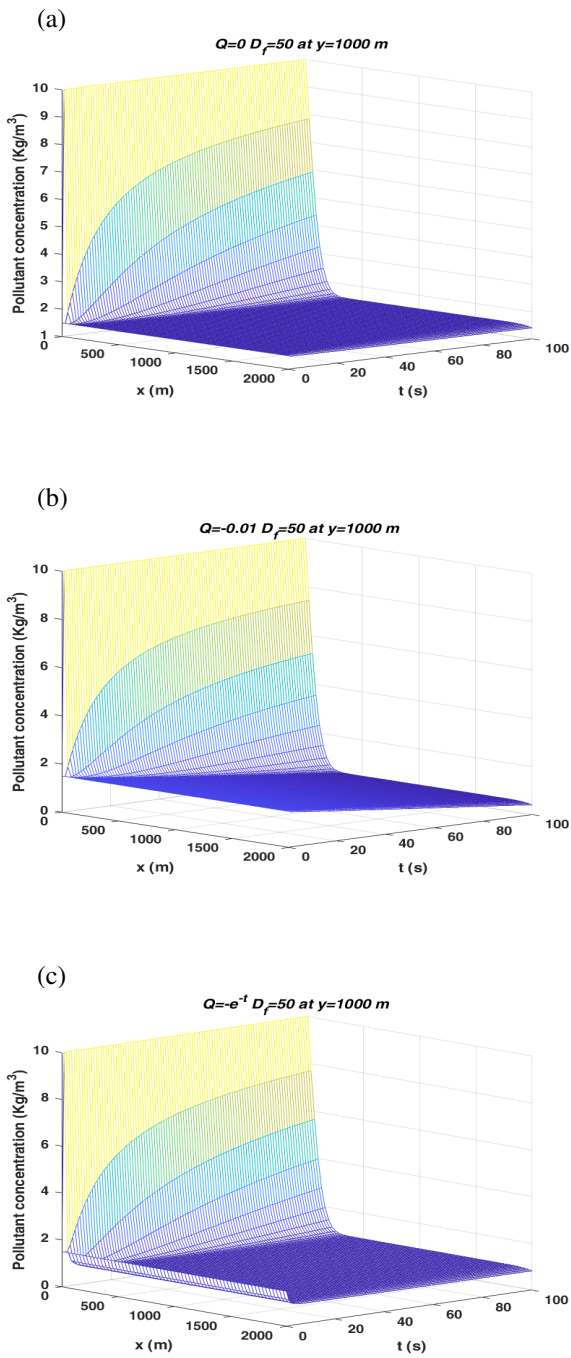


Fig. 13. The 3D graph of the approximated pollutant concentrations for one entrance gate case when $D_f = 50$, $y = 1000$ m and (a) $Q = 0$, (b) $Q = -0.01$ and (c) $Q = -e^{-t}$.

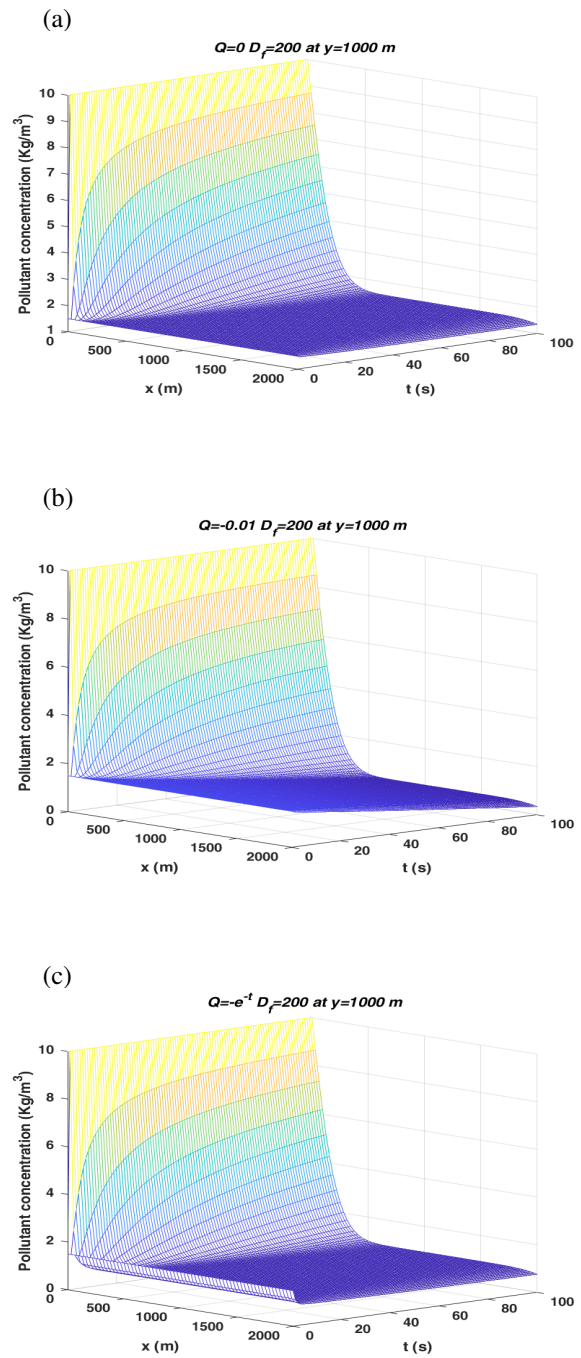


Fig. 14. The 3D graph of the approximated pollutant concentrations for one entrance gate case when $D_f = 200$, $y = 1000$ m and (a) $Q = 0$, (b) $Q = -0.01$ and (c) $Q = -e^{-t}$.

Comparison of pollutant concentration for $D_f=50$ at $x=125$ m and $y=1000$ m

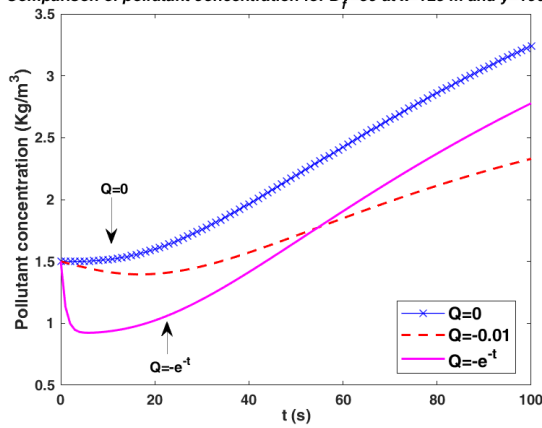


Fig. 15. Comparison of the pollutant concentrations for one entrance gate case when $D_f = 50$, $x = 125$, and $y = 1000$ m with $Q = 0$, $Q = -0.01$ and $Q = -e^{-t}$.

Comparison of pollutant concentration for $D_f=200$ at $x=125$ m and $y=1000$ m

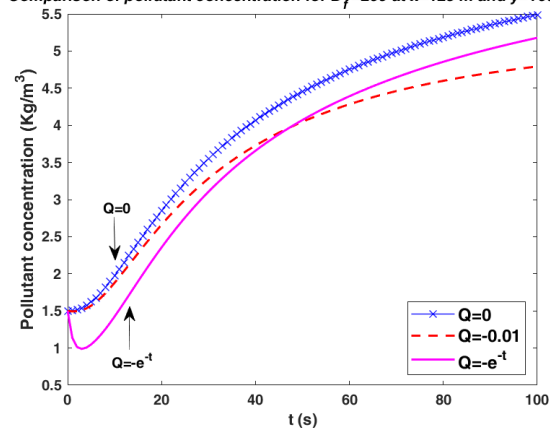


Fig. 17. Comparison of the pollutant concentrations for one entrance gate case when $D_f = 200$, $x = 125$, and $y = 1000$ m with $Q = 0$, $Q = -0.01$ and $Q = -e^{-t}$.

Comparison of pollutant concentration for $D_f=50$ at $x=250$ m and $y=1000$ m

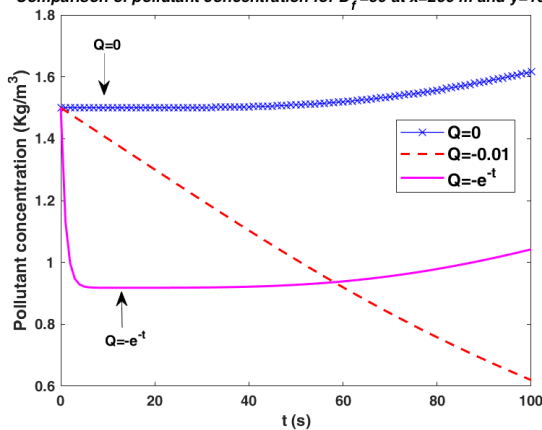


Fig. 16. Comparison of the pollutant concentrations for one entrance gate case when $D_f = 50$, $x = 250$, and $y = 1000$ m with $Q = 0$, $Q = -0.01$ and $Q = -e^{-t}$.

Comparison of pollutant concentration for $D_f=200$ at $x=250$ m and $y=1000$ m

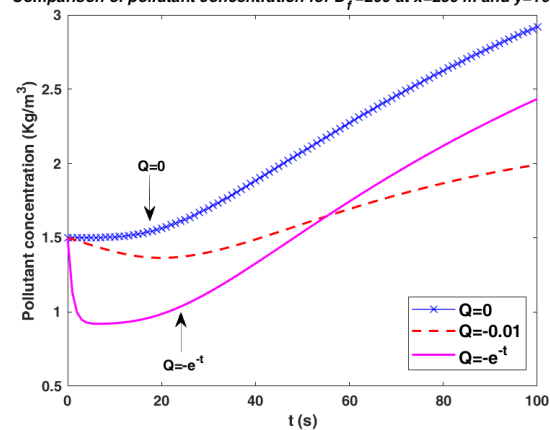


Fig. 18. Comparison of the pollutant concentrations for one entrance gate case when $D_f = 200$, $x = 250$, and $y = 1000$ m with $Q = 0$, $Q = -0.01$ and $Q = -e^{-t}$.

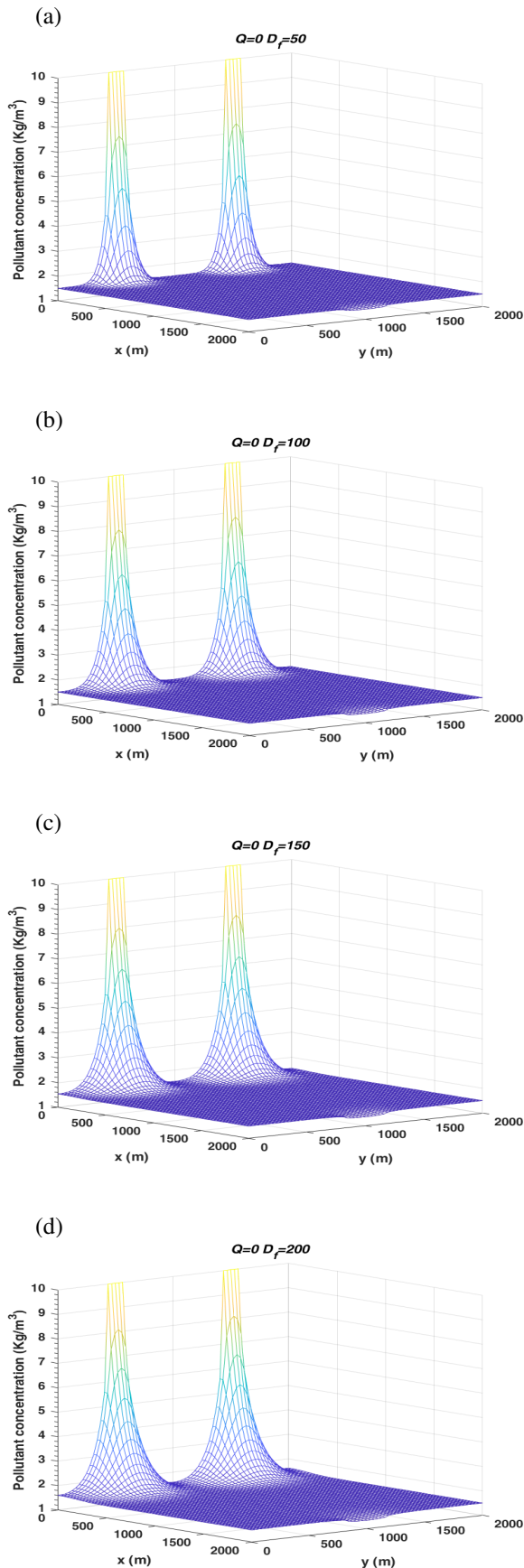


Fig. 19. The 3D graph of the approximated pollutant concentrations for two entrance gates case when $Q = 0$ and (a) $D_f = 50$, (b) $D_f = 100$, (c) $D_f = 150$ and (d) $D_f = 200$.

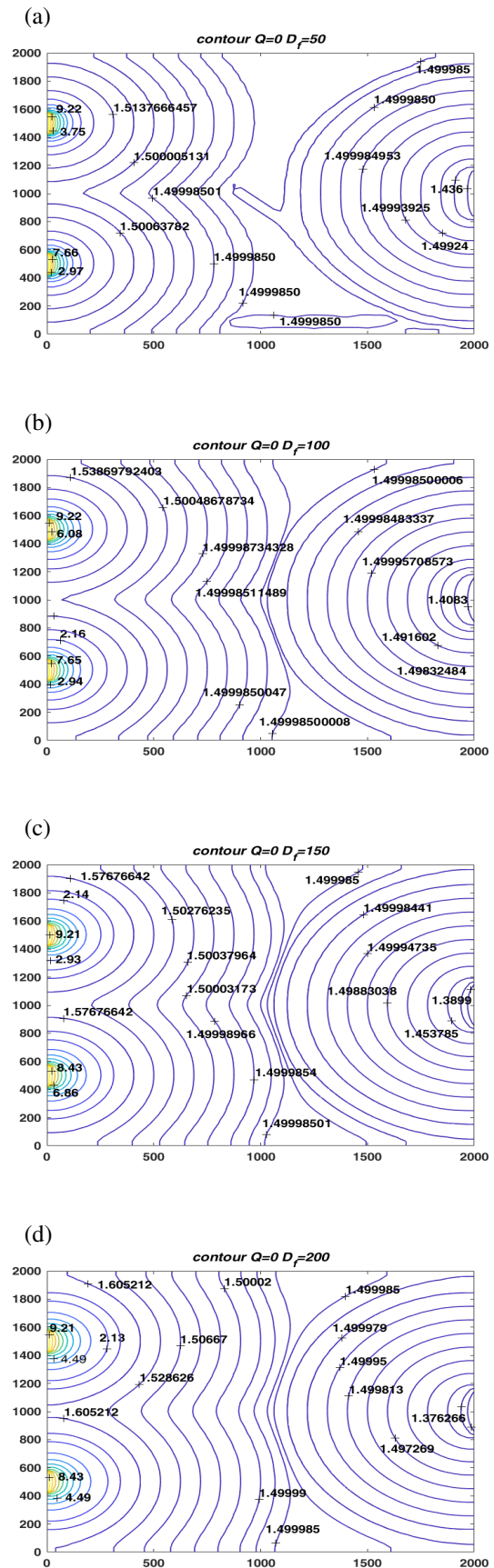


Fig. 20. The contour plots for two entrance gates case when $Q = 0$ and (a) $D_f = 50$, (b) $D_f = 100$, (c) $D_f = 150$ and (d) $D_f = 200$.

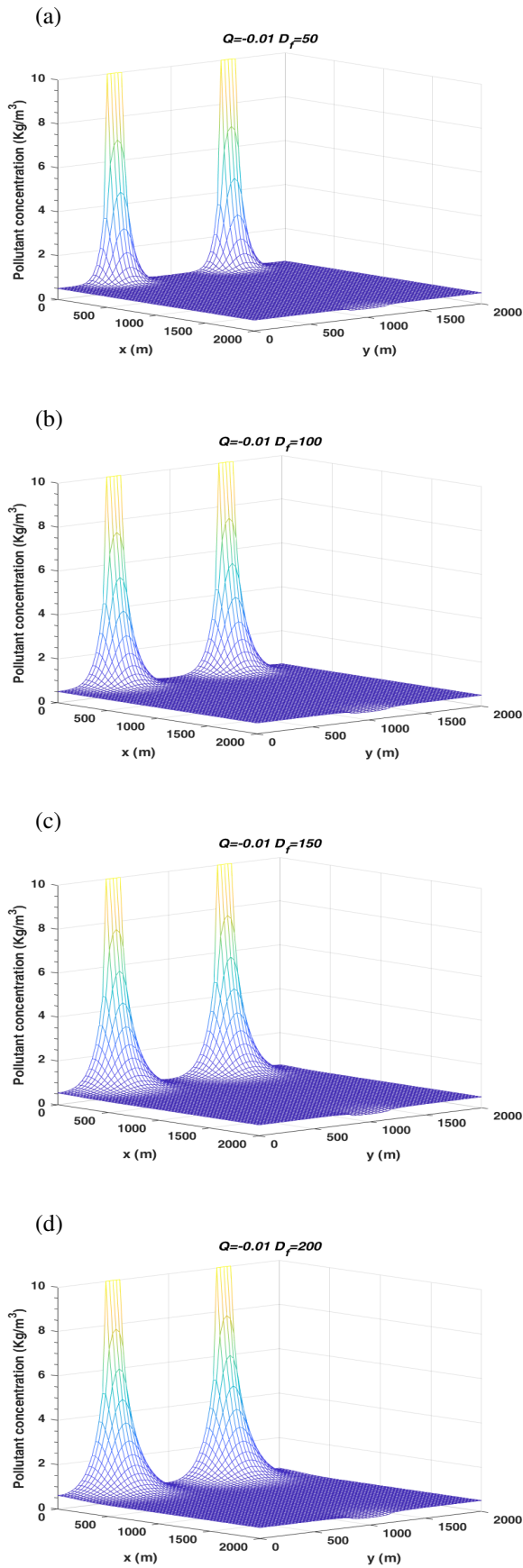


Fig. 21. The 3D graph of the approximated pollutant concentrations for two entrance gates case when $Q = -0.01$ and (a) $D_f = 50$, (b) $D_f = 100$, (c) $D_f = 150$ and (d) $D_f = 200$.

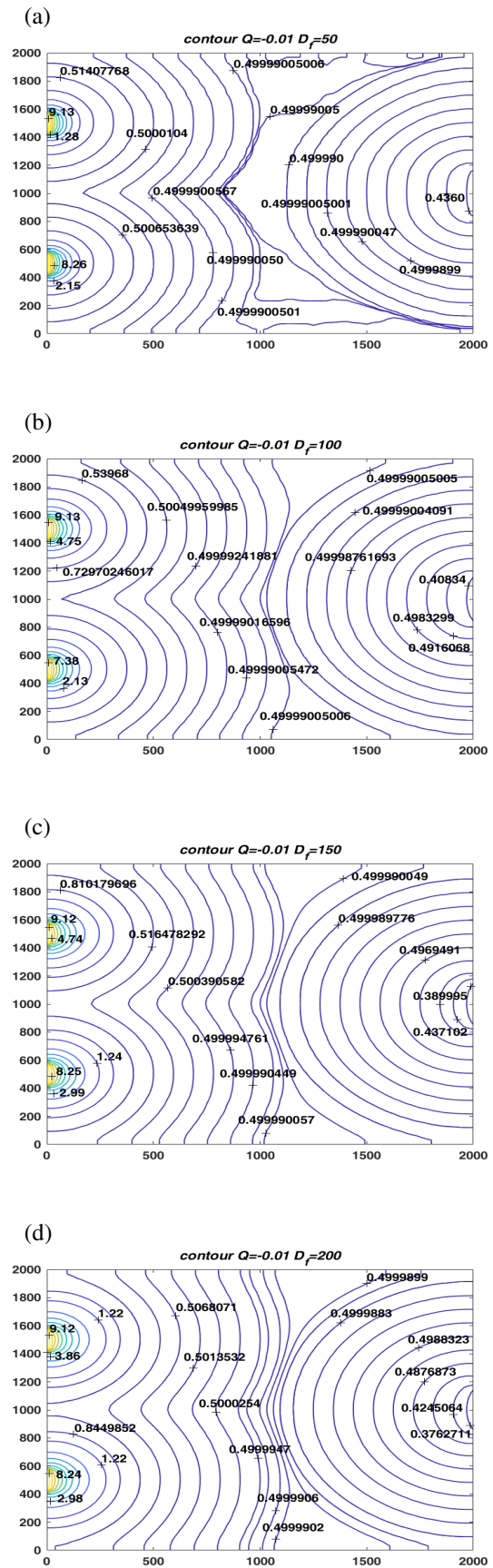


Fig. 22. The contour plots for two entrance gates case when $Q = -0.01$ and (a) $D_f = 50$, (b) $D_f = 100$, (c) $D_f = 150$ and (d) $D_f = 200$.

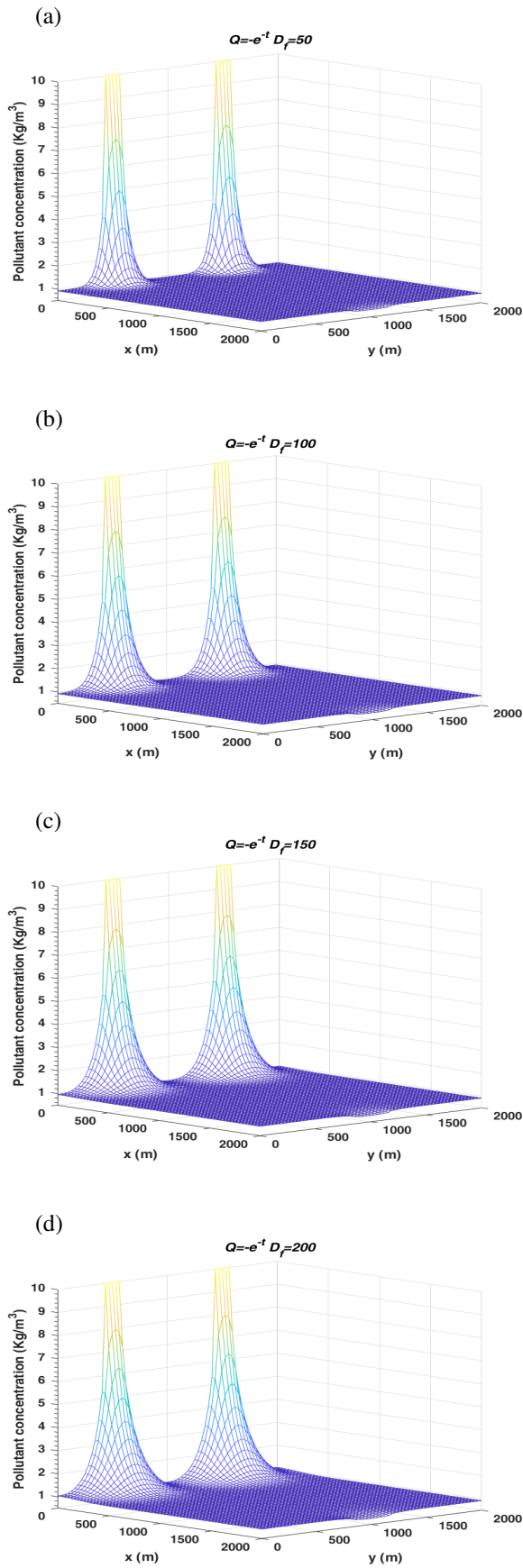


Fig. 23. The 3D graph of the approximated pollutant concentrations for two entrance gates case when $Q = -e^{-t}$ and (a) $D_f = 50$, (b) $D_f = 100$, (c) $D_f = 150$ and (d) $D_f = 200$.

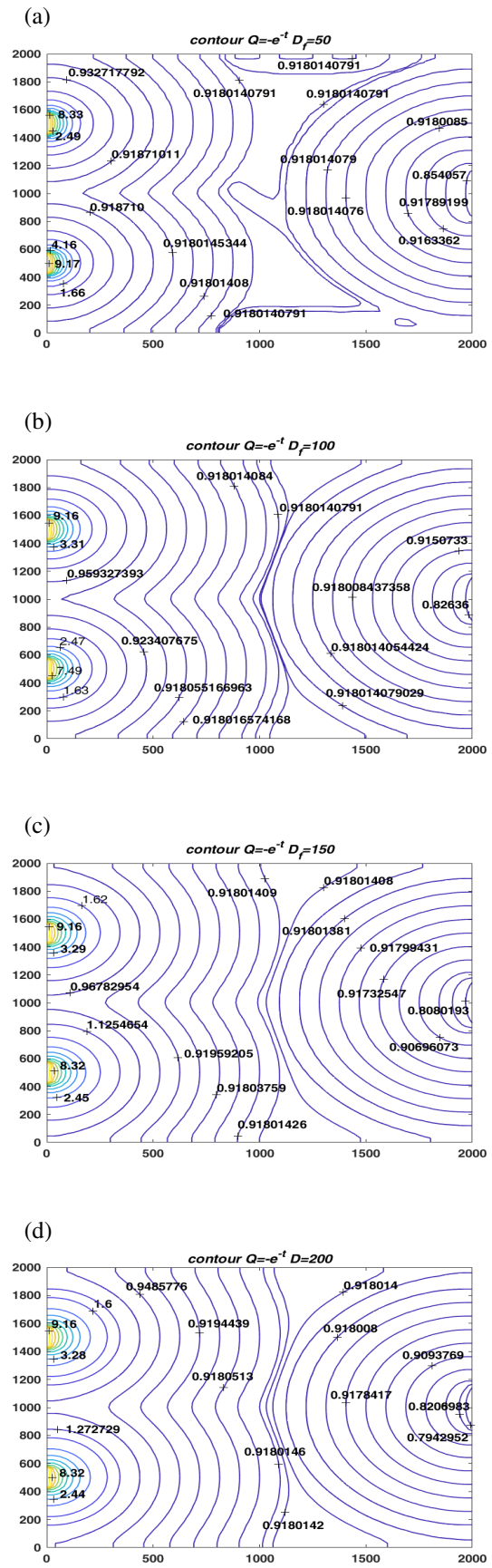


Fig. 24. The contour plots for two entrance gates case when $Q = -e^{-t}$ and (a) $D_f = 50$, (b) $D_f = 100$, (c) $D_f = 150$ and (d) $D_f = 200$.

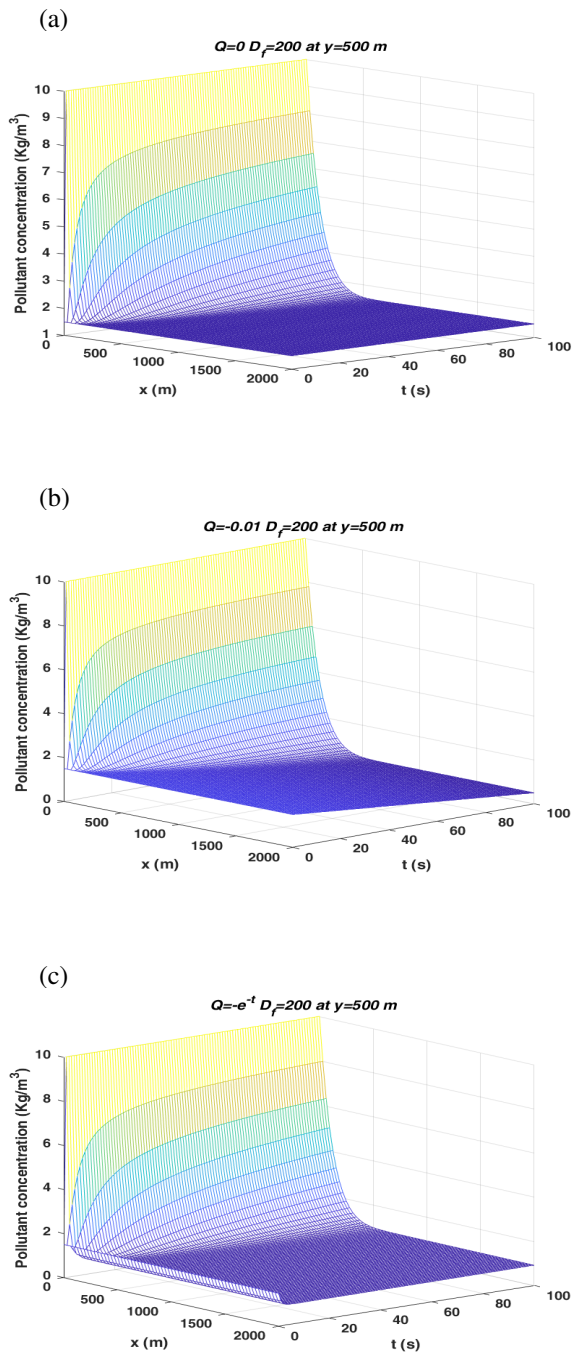


Fig. 25. The 3D graph of the approximated pollutant concentrations for two entrance gates case when $y = 500$ m and (a) $Q = 0$, (b) $Q = -0.01$ and (c) $Q = -e^{-t}$.

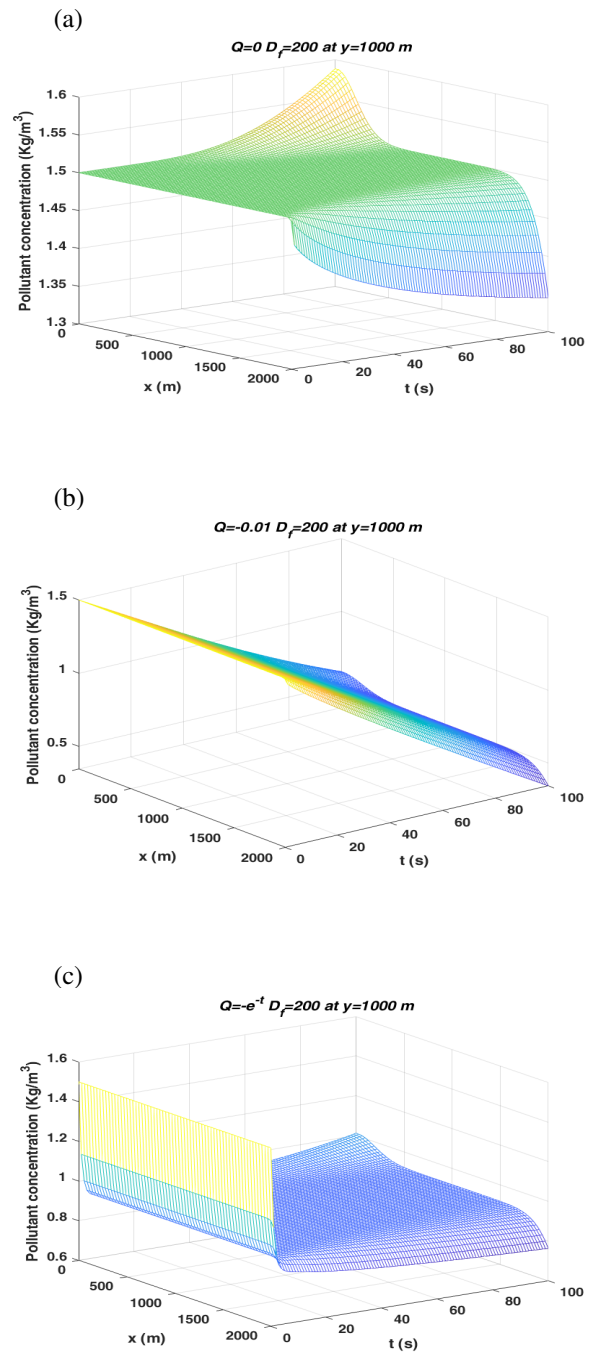


Fig. 26. The 3D graph of the approximated pollutant concentrations for two entrance gates case when $y = 1000$ m and (a) $Q = 0$, (b) $Q = -0.01$ and (c) $Q = -e^{-t}$.

Comparison of pollutant concentration for $D_f=200$ at $x=125$ m and $y=500$ m

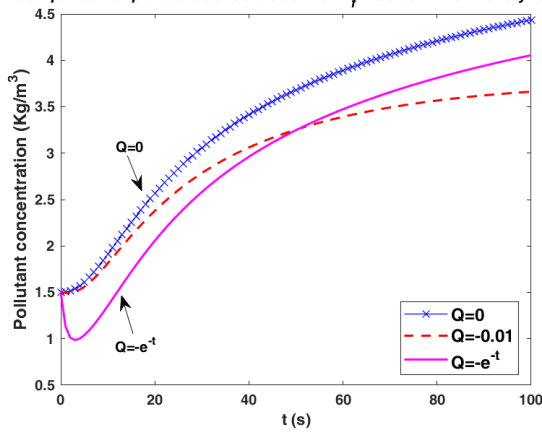


Fig. 27. Comparison of the pollutant concentrations for two entrance gates case when $D_f = 200$, $x = 125$, and $y = 500$ m with $Q = 0$, $Q = -0.01$ and $Q = -e^{-t}$.

Comparison of pollutant concentration for $D_f=200$ at $x=125$ m and $y=1000$ m

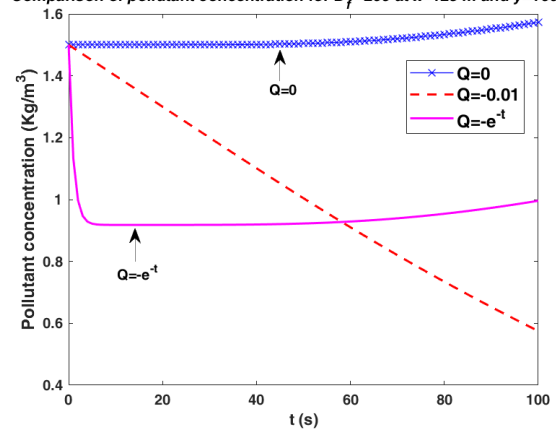


Fig. 29. Comparison of the pollutant concentrations for two entrance gates case when $D_f = 200$, $x = 125$, and $y = 1000$ m with $Q = 0$, $Q = -0.01$ and $Q = -e^{-t}$.

Comparison of pollutant concentration for $D_f=200$ at $x=250$ m and $y=500$ m

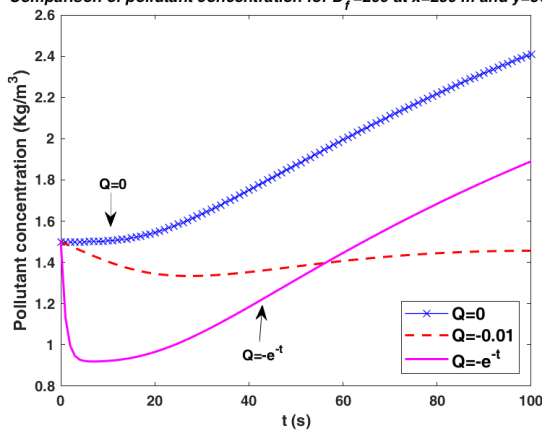


Fig. 28. Comparison of the pollutant concentrations for two entrance gates case when $D_f = 200$, $x = 250$, and $y = 500$ m with $Q = 0$, $Q = -0.01$ and $Q = -e^{-t}$.

Comparison of pollutant concentration for $D_f=200$ at $x=250$ m and $y=1000$ m

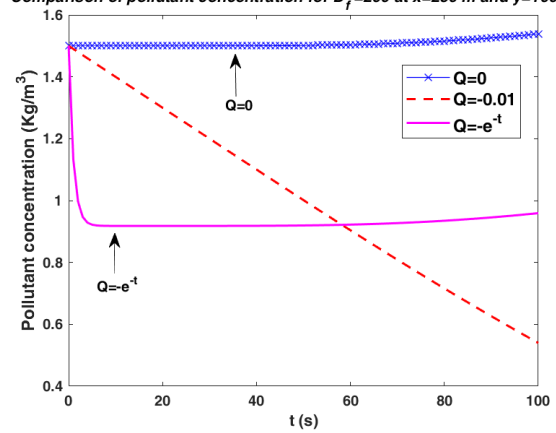


Fig. 30. Comparison of the pollutant concentrations for two entrance gates case when $D_f = 200$, $x = 250$, and $y = 1000$ m with $Q = 0$, $Q = -0.01$ and $Q = -e^{-t}$.

ACKNOWLEDGMENT

We would like to express my sincere thanks Department of Mathematics and Graduate College at King Mongkut's University of Technology North Bangkok for supporting us to do this research.

REFERENCES

- [1] Q. Feng, "Explicit finite difference method for convection-diffusion equations," in *Proceedings of the World Congress on Engineering*, vol. 2, 2009, pp. 1094–1097.
- [2] F. U. Prieto, J. J. B. Muñoz, and L. G. Corvinos, "Application of the generalized finite difference method to solve the advection–diffusion equation," *Journal of Computational and Applied Mathematics*, vol. 235, no. 7, pp. 1849–1855, 2011.
- [3] B. M. Chen-Charpentier and H. V. Kojouharov, "An unconditionally positivity preserving scheme for advection–diffusion reaction equations," *Mathematical and computer modelling*, vol. 57, no. 9–10, pp. 2177–2185, 2013.
- [4] A. R. Appadu, "Numerical solution of the 1d advection-diffusion equation using standard and nonstandard finite difference schemes," *Journal of Applied Mathematics*, vol. 2013, 2013.
- [5] A. Kaya, "A finite difference scheme for multidimensional convection–diffusion–reaction equations," *Computer Methods in Applied Mechanics and Engineering*, vol. 278, pp. 347–360, 2014.
- [6] L. Zhang, L. Wang, and X. Ding, "Exact finite difference scheme and nonstandard finite difference scheme for burgers and burgers-fisher equations," *Journal of Applied Mathematics*, vol. 2014, 2014.
- [7] A. Kaya, "Finite difference approximations of multidimensional unsteady convection–diffusion–reaction equations," *Journal of Computational Physics*, vol. 285, pp. 331–349, 2015.
- [8] A. Kaya and A. Sendur, "Finite difference approximations of multidimensional convection–diffusion–reaction problems with small diffusion on a special grid," *Journal of Computational Physics*, vol. 300, pp. 574–591, 2015.
- [9] F. Sanjaya and S. Mungkasi, "A simple but accurate explicit finite difference method for the advection-diffusion equation," in *Journal of Physics: Conference Series*, vol. 909, no. 1. IOP Publishing, 2017, pp. 012–038.
- [10] K. Suebyat and N. Pochai, "A numerical simulation of a three-dimensional air quality model in an area under a bangkok sky train platform using an explicit finite difference scheme," *IAENG International Journal of Applied Mathematics*, vol. 47, no. 4, pp. 471–476, 2017.
- [11] R. Company, V. N. Egorova, and L. Jódar, "Conditional full stability of positivity-preserving finite difference scheme for diffusion–advection–reaction models," *Journal of Computational and Applied Mathematics*, vol. 341, pp. 157–168, 2018.
- [12] P. Lenarda, M. Paggi, and R. R. Baier, "Partitioned coupling of advection–diffusion–reaction systems and brinkman flows," *Journal of Computational Physics*, vol. 344, pp. 281–302, 2017.
- [13] S. Phongthanapanich and P. Dechaumphai, "Finite volume method for convection–diffusion–reaction equation on triangular meshes," *International Journal for Numerical Methods in Biomedical Engineering*, vol. 26, no. 6, pp. 716–727, 2010.
- [14] S. Phongthanapanich and P. Dechaumphai, "Explicit characteristic finite volume method for convection–diffusion equation on rectangular grids," *Journal of the Chinese Institute of Engineers*, vol. 34, no. 2, pp. 239–252, 2011.
- [15] A. Tambue, "An exponential integrator for finite volume discretization of a reaction–advection–diffusion equation," *Computers & Mathematics with Applications*, vol. 71, no. 9, pp. 1875–1897, 2016.
- [16] Z. Lin and Q. Zhang, "High-order finite-volume solutions of the steady-state advection–diffusion equation with nonlinear robin boundary conditions," *Journal of Computational Physics*, vol. 345, pp. 358–372, 2017.
- [17] M. Xu, "A modified finite volume method for convection-diffusion-reaction problems," *International Journal of Heat and Mass Transfer*, vol. 117, pp. 658–668, 2018.
- [18] S. Reutskiy and J. Lin, "A meshless radial basis function method for steady-state advection-diffusion-reaction equation in arbitrary 2d domains," *Engineering Analysis with Boundary Elements*, vol. 79, pp. 49–61, 2017.
- [19] M. Gharib, M. Khezri, and S. Foster, "Meshless and analytical solutions to the time-dependent advection-diffusion-reaction equation with variable coefficients and boundary conditions," *Applied Mathematical Modelling*, vol. 49, pp. 220–242, 2017.
- [20] M. Gharib, M. Khezri, S. Foster, and A. Castel, "Application of the meshless generalised rkpm to the transient advection-diffusion-reaction equation," *Computers & Structures*, vol. 193, pp. 172–186, 2017.
- [21] J. Lin and S. Reutskiy, "An accurate meshless formulation for the simulation of linear and fully nonlinear advection diffusion reaction problems," *Advances in Engineering Software*, 2018.
- [22] J. Lin, S. Reutskiy, and J. Lu, "A novel meshless method for fully nonlinear advection–diffusion–reaction problems to model transfer in anisotropic media," *Applied Mathematics and Computation*, vol. 339, pp. 459–476, 2018.
- [23] M. Siddique, "Numerical computation of two-dimensional diffusion equation with nonlocal boundary conditions," *IAENG International Journal of Applied Mathematics*, vol. 40, no. 1, pp. 26–31, 2010.
- [24] L. Qian and H. Cai, "Implicit-explicit time stepping scheme based on the streamline diffusion method for fluid-fluid interaction problems," *IAENG International Journal of Applied Mathematics*, vol. 48, no. 3, pp. 278–287, 2018.
- [25] D. Anderson, J. C. Tannehill, and R. H. Pletcher, *Computational fluid mechanics and heat transfer*. CRC Press, 2016.
- [26] M. Dehghan, "Weighted finite difference techniques for the one-dimensional advection–diffusion equation," *Applied Mathematics and Computation*, vol. 147, no. 2, pp. 307–319, 2004.
- [27] A. Mohammadi, M. Manteghian, and A. Mohammadi, "Numerical solution of the one-dimensional advection-diffusion equation using simultaneously temporal and spatial weighted parameters," *Australian Journal of Basic and Applied Sciences*, vol. 5, no. 6, pp. 1536–1543, 2011.
- [28] P. Samalerk and N. Pochai, "Numerical simulation of a one-dimensional water-quality model in a stream using a saulyev technique with quadratic interpolated initial-boundary conditions," in *Abstract and Applied Analysis*, vol. 2018. Hindawi, 2018.
- [29] N. Pochai and R. Deepana, "A numerical computation of water quality measurement in a uniform channel using a finite difference method," *Procedia Engineering*, vol. 8, pp. 85–88, 2011.
- [30] N. Pochai, "Numerical treatment of a modified maccormack scheme in a nondimensional form of the water quality models in a nonuniform flow stream," *Journal of Applied Mathematics*, vol. 2014, 2014.
- [31] W. Kraychang and N. Pochai, "Numerical treatment to a water-quality measurement model in an opened-closed reservoir," *Thai Journal of Mathematics*, vol. 13, no. 3, pp. 775–788, 2016.
- [32] W. Kraychang and N. Pochai, "Implicit finite difference simulation of water pollution control in a connected reservoir system," *IAENG International Journal of Applied Mathematics*, vol. 46, no. 1, pp. 47–57, 2016.
- [33] K. Thongtha and J. Kasemsuwan, "Numerical simulations of water quality measurement model in an opened-closed reservoir with contaminant removal mechanism," *International Journal of Differential Equations*, vol. 2018, 2018.